ACS NANO

www.acsnano.org

ARTICLE

Mucoadhesive Tannic Acid-Cross-Linked Nanogels for Reactive Oxygen Species Scavenging and Enhanced Ocular Therapeutic Delivery

Yavuz Oz,[#] Yuting Zheng,[#] Prince Kumar, Lal Krishan Kumar, Arpita Roy, Iris Qi, Zhanpeng Jim Liu, Pawan Kumar Singh, and Nasim Annabi*

Cite This: *ACS Nano* 2025, 19, 27173–27191

Read Online

ACCESS | Metrics & More | Article Recommendations | Supporting Information

ABSTRACT: **Mucoadhesive nanoparticles show promise for mucosal drug delivery, but ocular applications remain limited by rapid clearance, poor retention, and insufficient drug encapsulation. Existing systems struggle to deliver a full spectrum of therapeutics, hydrophobic drugs, hydrophilic drugs, and proteins, despite the critical need for such versatility in treating complex ocular diseases. Many eye conditions, including infection, inflammation, and degenerative disorder, require combination therapies or multidrug regimens for optimal therapeutic outcomes. To address these limitations, we developed a biocompatible tannic acid (TA)-cross-linked nanogel (NG) platform with robust mucoadhesion, anti-inflammatory, reactive oxygen species (ROS) scavenging properties, and sustained drug-release capabilities. The NGs were synthesized from a temperature-responsive poly(ethylene glycol)-based copolymer that self-aggregates above its lower critical solution temperature and is cross-linked with TA. TA's polyphenolic structure enables multimodal mucoadhesion and antioxidant activity, enhancing ocular retention and protecting against ROS-induced damage. The NGs achieved high loading efficiency (>80%) for diverse therapeutics, including moxifloxacin, a hydrophilic antibiotic; dexamethasone (Dex), a hydrophobic anti-inflammatory drug; as well as bovine serum albumin, used as a model protein to explore potential for protein encapsulation. In proof-of-concept studies, Dex-loaded NGs demonstrated sustained release (>24 days) and therapeutic efficacy *in vitro* and *in vivo*. Blank NGs also exhibited anti-inflammatory activity *in vivo*, comparable to Dex-loaded NGs in an acute model of ocular inflammation, demonstrating their intrinsic therapeutic potential. By enabling delivery of multiple therapeutic classes while providing inherent anti-inflammatory function, this TA-cross-linked NG platform offers a versatile and effective strategy for managing complex ocular diseases.**

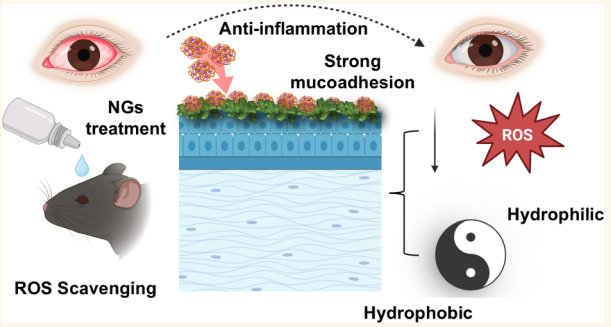

KEYWORDS: *nanogels, mucoadhesive, drug delivery, ROS-scavenging, inflammation, retina, eye*

INTRODUCTION

Mucoadhesive nanoparticles (NPs) have emerged as potential candidates for nanomedicine, targeting various diseases occurring in tissues coated with mucosal surfaces, including those of the ocular, vaginal, intestinal, lung and nasal regions.[1−4] Among these mucosal surfaces, the use of mucoadhesive NPs for therapeutics delivery is particularly critical for treating ocular diseases due to persistent challenges such as tear turnover and blinking reflex, which leave less than 5% of the active drug on the ocular surface.[5] Although recent advancements have led to the development of mucoadhesive NPs for ocular drug delivery, several challenges remain. For instance, mucoadhesive functional groups such as phenylboronic acid (PBA)[6−8] and thiols[9] have been conjugated to NPs, facilitating covalent interactions between the NPs and mucin. However, these interactions are influenced by various factors, such as pH, water content, or temperature, which can weaken the binding of these NPs to mucin. Another limitation of these mucoadhesive NPs is their inability to encapsulate a

Received: February 3, 2025
Revised: July 8, 2025
Accepted: July 9, 2025
Published: July 23, 2025

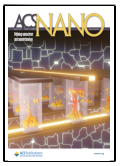

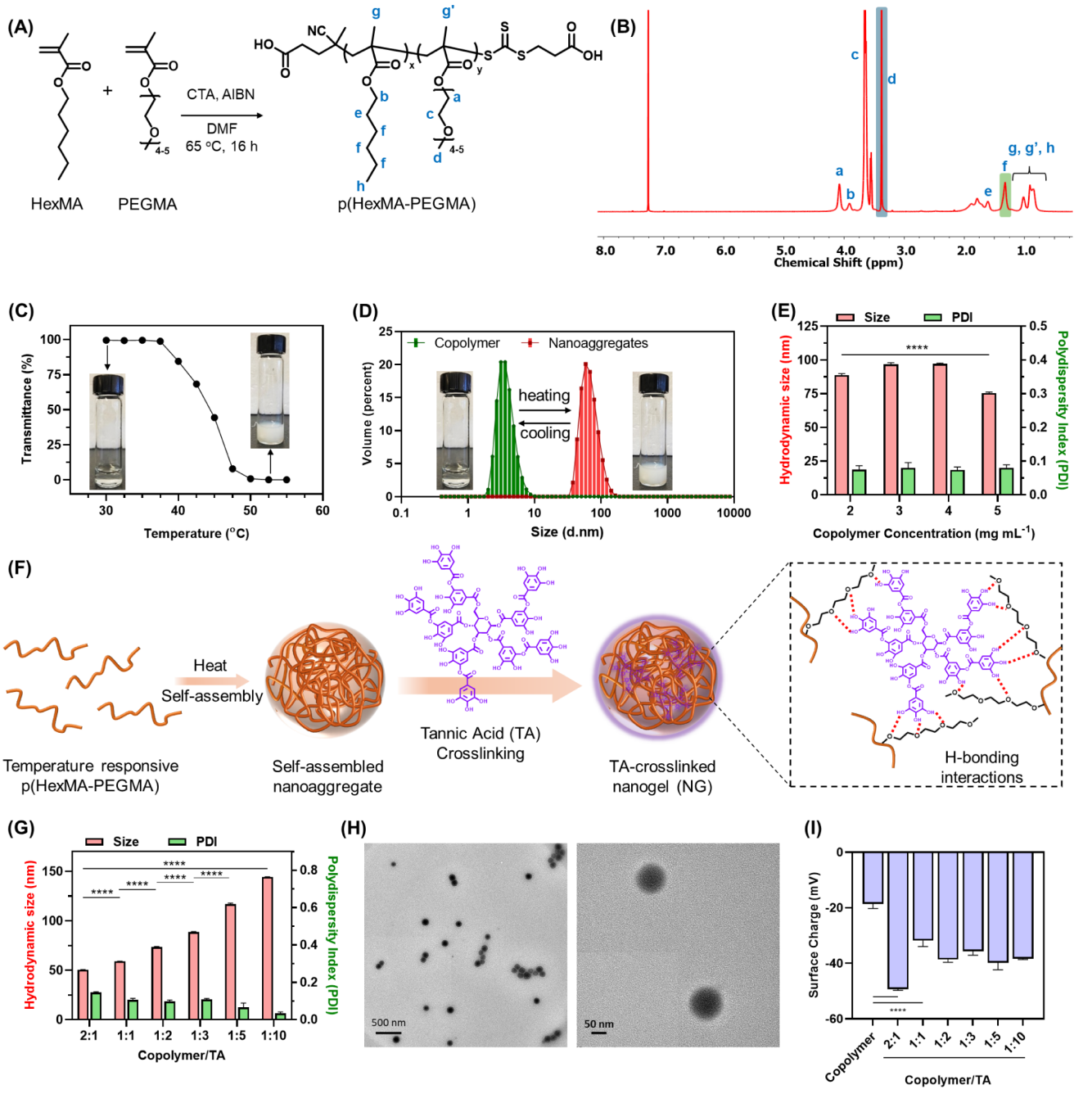

Figure 1. Formation and characterization of TA-cross-linked NGs. (A) Synthesis of p(HexMA-PEGMA) copolymer via a RAFT polymerization; (B) ^{1}H NMR spectrum of p(HexMA-PEGMA) copolymer; (C) % transmittance change of p(HexMA-PEGMA) copolymer solution with temperature; (D) hydrodynamic size change of the copolymer upon heating and cooling, determined by DLS; (E) hydrodynamic size and PDI of nanoaggregates at 55 °C with varying copolymer concentrations; (F) physical cross-linking of self-assembled copolymer by TA to form NGs through H-bonding interactions between TA and PEG; (G) hydrodynamic size and PDI of cross-linked NGs formed with different copolymer/TA ratios at 25 °C; (H) representative TEM images of NGs; (I) zeta potential of NG solutions formed at different copolymer/TA ratio.

wide range of therapeutic agents, including hydrophilic drugs, hydrophobic drugs, and small/large proteins. This constraint is particularly important in cases where combination therapy is essential for effectively treating eye diseases such as ocular neovascularization.[10] Therefore, there is an urgent need to develop an ocular drug delivery system that provides both strong mucoadhesion properties as well as the ability to provide sustained delivery of a wide range of therapeutics.

Nanogels (NGs) have recently garnered significant interest as drug delivery vehicles due to their capacity to load both hydrophobic and hydrophilic drugs, as well as various biomolecules.[11] They also offer adjustable sizes[12] and the possibility of using a wide range of polymers for their synthesis,[13] providing flexibility in designing mucoadhesive drug delivery systems tailored for the treatment of specific ocular diseases. For example, natural polymers such as chitosan (CS) and hyaluronic acid (HA) are widely used in designing

https://doi.org/10.1021/acsnano.5c02002
ACS Nano 2025, 19, 27173−27191

NGs for ocular delivery due to their intrinsic mucoadhesive properties.[14−16] However, recent research has shifted toward CS derivatives with additional mucoadhesive groups, such as maleimide, thiol, and PBA, which offer enhanced mucoadhesion compared to unmodified CS.[6,17,18] Despite their advantages, these derivatives have limitations, including the need for chemical modifications and the low stability of their functional groups, which may hinder long-term effectiveness. For instance, PBA-based boronate esters hydrolyze in neutral to acidic environments, maleimide groups are prone to hydrolysis above pH 5.5 and can undergo reversible Michael addition, and thiol groups may oxidize or self-cross-link, affecting long-term performance.[19−22] These issues underscore the challenge of balancing strong mucoadhesion with chemical stability for sustained ocular drug delivery. Similarly, HA requires modification with hydrophobic molecules such as cholesterol to enable self-assembly into NGs.[16,23] This hydrophobic modification also facilitates the loading of both hydrophilic and hydrophobic drugs for ocular delivery. Zoratto *et al.* demonstrated that cholesterol-modified HA, cross-linked using an autoclaving method at 121 °C, improved the ocular delivery of both hydrophilic and hydrophobic drugs.[16] However, the high temperature required for NG formation may not be suitable for biomolecule loading, as it can compromise the therapeutic activity of biomolecules. Although limited research has explored the use of synthetic polymers for engineering NGs in ocular delivery, polymers such as polyvinylpyrrolidone, poly(acrylic acid), and 2-hydroxyethyl methacrylate have been utilized to develop NGs for this purpose.[24,25] However, NGs made from synthetic polymers lacked the inherent mucoadhesive properties of CS and HA, making them less effective at overcoming common ocular drug delivery challenges. Therefore, there is a need for engineering an effective delivery system that can address challenges such as the requirement for polymer modifications to achieve amphiphilicity or mucoadhesiveness, harsh reaction conditions, and the limited choice of therapeutics. The use of temperature-responsive copolymers that form nanoaggregates upon mild heating, followed by tannic acid (TA) stabilization, could provide the necessary mucoadhesive properties, eliminating the need for chemical modifications while offering good stability and the ability to load various therapeutic agents.

The polyphenolic structure of natural TA exhibits strong mucoadhesive characteristics due to covalent bonding, hydrogen bonding (H-bonding) and hydrophobic interactions with the mucus layer.[26−28] This multi-interaction mechanism, which combines both covalent and noncovalent bonding, enhances the stability and retention of NGs on the ocular surface. Furthermore, the antioxidant properties of TA could be harnessed to combat the increase in reactive oxygen species (ROS) associated with various ocular diseases.[29,30] Recent studies show that degenerative and inflammatory eye conditions, such as age-related macular degeneration,[31] diabetic retinopathy,[32] cataracts,[33] glaucoma,[34] and uveitis,[35] are associated with increased ROS production in the eye and subsequent damage to ocular tissues. Therefore, designing TA-cross-linked NGs may present a versatile drug delivery platform capable of delivering a broad range of therapeutics with enhanced mucoadhesion and ROS-scavenging ability for the treatment of these ocular diseases. In contrast, existing mucoadhesive NPs are often designed to deliver specific therapeutics for particular ocular diseases and typically necessitate a combination therapy or codelivery of drugs to achieve effective treatment—a challenge that TA-cross-linked NGs can readily address. While TA has been widely utilized in engineering polymer-based NPs for its antioxidant and antibacterial properties, its potential as a mucoadhesive agent in ocular drug delivery remains largely unexplored.[36−39]

Considering the limitations of current ocular drug delivery systems, in this study, we engineered mucoadhesive and ROS-scavenging NGs that can deliver either hydrophobic and hydrophilic drugs or therapeutic proteins for the treatment of ocular inflammation. A temperature-responsive poly(ethylene glycol) (PEG)-based copolymer was synthesized, which self-aggregated above its lower critical solution temperature (LCST) and cross-linked with TA through H-bonding interactions. This simple yet effective approach imparted the NGs with both antioxidant and mucoadhesive properties due to the presence of TA, as evaluated *in vitro*. As proof of concept, a well-known anti-inflammatory drug, dexamethasone (Dex), was encapsulated within the NGs and their therapeutic efficacy was tested using an *in vivo* lipopolysaccharide (LPS)-induced intraocular inflammation model. The engineered TA-cross-linked mucoadhesive NGs, capable of loading various therapeutic agents, demonstrated their potential as a vehicle for effective intraocular drug delivery, aiming to achieve improved therapeutic outcomes for a broad spectrum of ocular diseases.

RESULTS AND DISCUSSION

Synthesis and Characterization of p(HexMA-PEGMA) and TA-Cross-Linked NGs. The one-step synthesis of poly(hexyl methacrylate-*co*-poly(ethylene glycol) methyl ether methacrylate) (p(HexMA-PEGMA)) copolymer was accomplished using reversible addition−fragmentation chain transfer (RAFT) polymerization. Hexyl methacrylate (HexMA) and poly(ethylene glycol) methyl ether methacrylate (PEGMA) monomers were polymerized in the presence of a RAFT agent at 65 °C for 16 h, initiated by azobis-(isobutyronitrile) (AIBN) (Figure 1A). The number-average molecular weight (M_n) of the p(HexMA-PEGMA) copolymer was determined to be 17 100 g/mol with a dispersity (M_w/M_n) of 1.25, as measured by size exclusion chromatography (SEC) (Figure S1). The successful polymerization was verified by proton nuclear magnetic resonance (^{1}H NMR) spectroscopy, which revealed the proton resonance of the terminal methyl ether group of the PEGMA monomer at 3.38 ppm (blue highlighted peak) and the pendant methylene ($-CH_2-$) groups of HexMA at 1.32 ppm (green highlighted peak) (Figure 1B). The hydrophilic PEGMA monomer was chosen for its thermoresponsive ethylene glycol pendant groups, which facilitate the formation of nanoaggregates above their LCST.[40−42] To form stable NGs with TA cross-linking, we first determined the LCST of the p(HexMA-PEGMA) copolymer by turbidimetry measurement using ultraviolet−visible (UV−vis) spectroscopy. An aqueous solution of copolymer (5 mg/mL) was heated from 30 to 55 °C, and the absorbance of the solution was measured at 600 nm at 2.5 °C intervals. This wavelength is commonly used for NP turbidity measurements, as it minimizes interference from sample components while effectively capturing particle-induced light scattering.[41,43] The transmittance of the solution was calculated using absorbance values to determine the LCST of the copolymer solution. The LCST of p(HexMA-PEGMA) copolymer solution was found to be 45 °C from the transmittance-temperature curve (Figure 1C). Above this temperature, the p(HexMA-PEGMA) copolymer formed

https://doi.org/10.1021/acsnano.5c02002
ACS Nano 2025, 19, 27173−27191

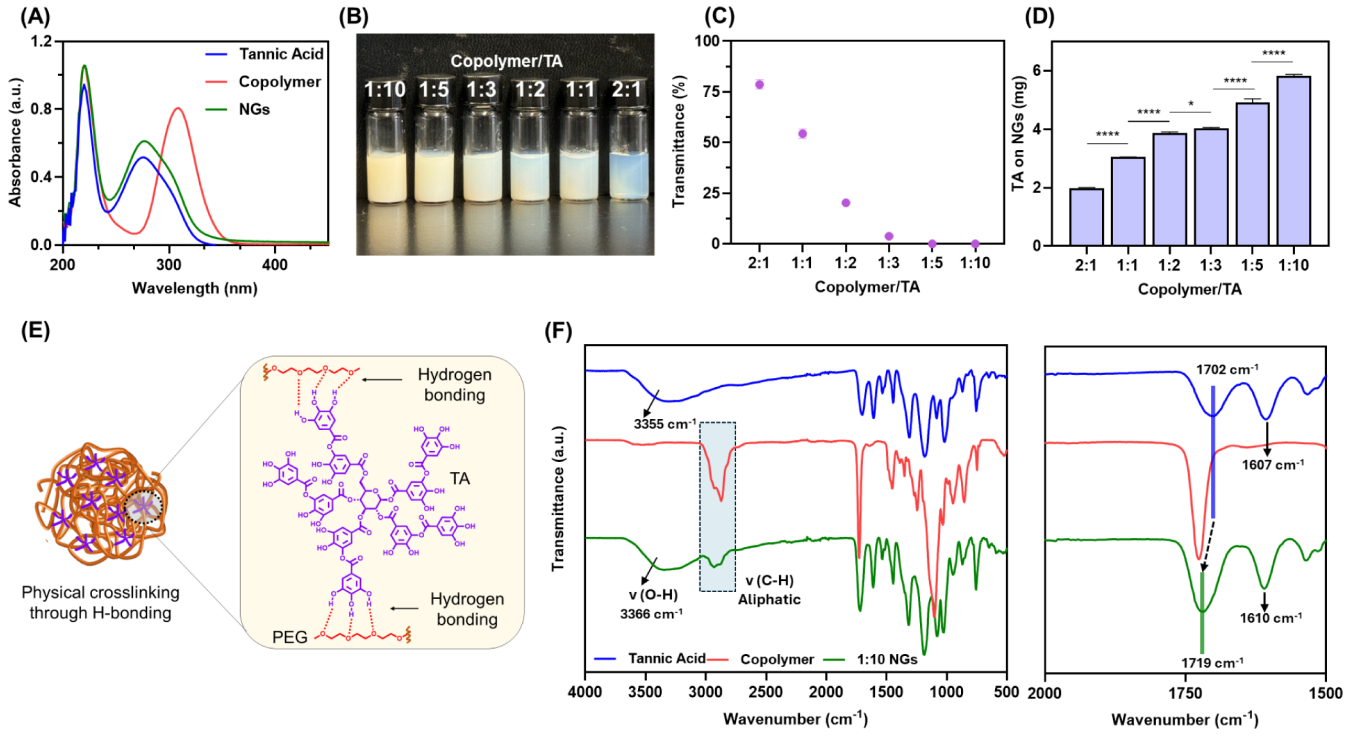

Figure 2. Characterization of TA incorporation and H-bonding interactions with the copolymer. (A) UV−vis spectrum of p(HexMA-PEGMA) copolymer, TA and 1:10 NGs; (B) representative images of NG solutions with varying ratios of copolymer and TA; (C) % transmittance change of NGs formed by using different copolymer/TA ratios; (D) the amount of TA in 5 mg/mL NGs solution; (E) possible interactions between copolymer and TA in NGs and (F) FTIR spectra of TA, copolymer, and physically cross-linked NGs.

nanosized aggregates in water. The size of these nanoaggregates was around 75.5 nm at 55 °C indicated by dynamic light scattering (DLS), while the size of entangled copolymer chains in the solution was 8.7 nm at room temperature (Figure 1D). It was observed that heating the solution to 55 °C triggered polymer chains to aggregate, forming a turbid solution, while the solution became transparent again upon cooling (Figure 1D). This observation indicated that cross-linking was essential for stabilizing the nanoaggregates in solution at 25 °C, as the polymer chains dissolved back into the water at this temperature. To determine if the copolymer concentration affects the hydrodynamic size and polydispersity index (PDI) of nanoaggregates, we prepared p(HexMA-PEGMA) copolymer solutions in water at varying concentrations of 2, 3, 4, and 5 mg/mL, heated them to 55 °C, and analyzed their sizes and PDIs using DLS. While the PDI of all NGs was around ∼0.08, the hydrodynamic sizes dropped from 88.7 ± 0.9 nm to 75.5 ± 0.5 nm by increasing the concentration from 2 to 5 mg/mL (Figure 1E). This could be due to stronger interactions between polymer chains at higher concentrations at 55 °C.[44] At this temperature, hydrogen bonds between water molecules and PEG break, making PEG more hydrophobic. As a result, stronger intermolecular hydrophobic interactions promote the formation of nanoaggregates.[45]

Ethylene glycol groups of the copolymer strongly interact with polyols via H-bonding interactions.[46−48] Therefore, TA was used to cross-link the nanoaggregates formed by heating the p(HexMA-PEGMA) copolymer solution, as phenolic −OH groups of TA could strongly interact with the ethylene glycol ($-CH_2CH_2O-$) groups in PEGMA through H-bonding (Figure 1F). The cross-linked structure of NGs makes them an essential tool for drug delivery applications, providing long-term stability. We selected the nanoaggregates with the smallest hydrodynamic size obtained by 5 mg/mL copolymer solution for cross-linking, as their higher surface area could facilitate more interactions with TA during cross-linking.[49] The formation of NGs was examined by mixing the p(HexMA-PEGMA) copolymer with TA in various ratios at 55 °C. Initially, nanoaggregates were cross-linked using a 3:1 copolymer/TA ratio; however, these NGs were unstable upon cooling to room temperature, likely due to insufficient cross-linking. Then, at a fixed copolymer concentration of 5 mg/mL, the copolymer/TA ratio was changed from 2:1 to 1:10 to form NGs at 55 °C. The hydrodynamic sizes of NGs increased from 50.4 ± 0.2 nm to 144.3 ± 0.2 nm with higher TA ratios, while PDI values decreased, reaching a minimum of 0.03 ± 0.01 at a 1:10 copolymer/TA ratio (Figure 1G). The increase in the hydrodynamic size of the NGs could be attributed to the incorporation of additional polymer chains during formation of nanoaggregates, facilitated by the higher TA content interacting with the polymer chains. The decrease in PDI with higher TA ratios may be attributed to increased cross-linking density, leading to more robust NG structures. Additionally, the higher TA content may enhance electrostatic repulsion, reducing NG aggregation and contributing to a more uniform NG distribution. Further increase in TA ratio to 1:20 resulted in the formation of large aggregates (3.4 μm) with a high PDI of 0.7 (Figure S2A). The TEM characterization of NGs with a 1:10 ratio revealed that they were spherical, with an average size of 116 ± 13 nm (Figure 1H). It is also crucial to maintain the size of the NGs below 500 nm to ensure efficient mucoadhesion and facilitate particle diffusion through the mucus layer. If the NGs are larger than 500 nm, steric hindrance will prevent them from diffusing through the mucus layer effectively.[50] The zeta potentials of the p(HexMA-

https://doi.org/10.1021/acsnano.5c02002
ACS Nano 2025, 19, 27173−27191

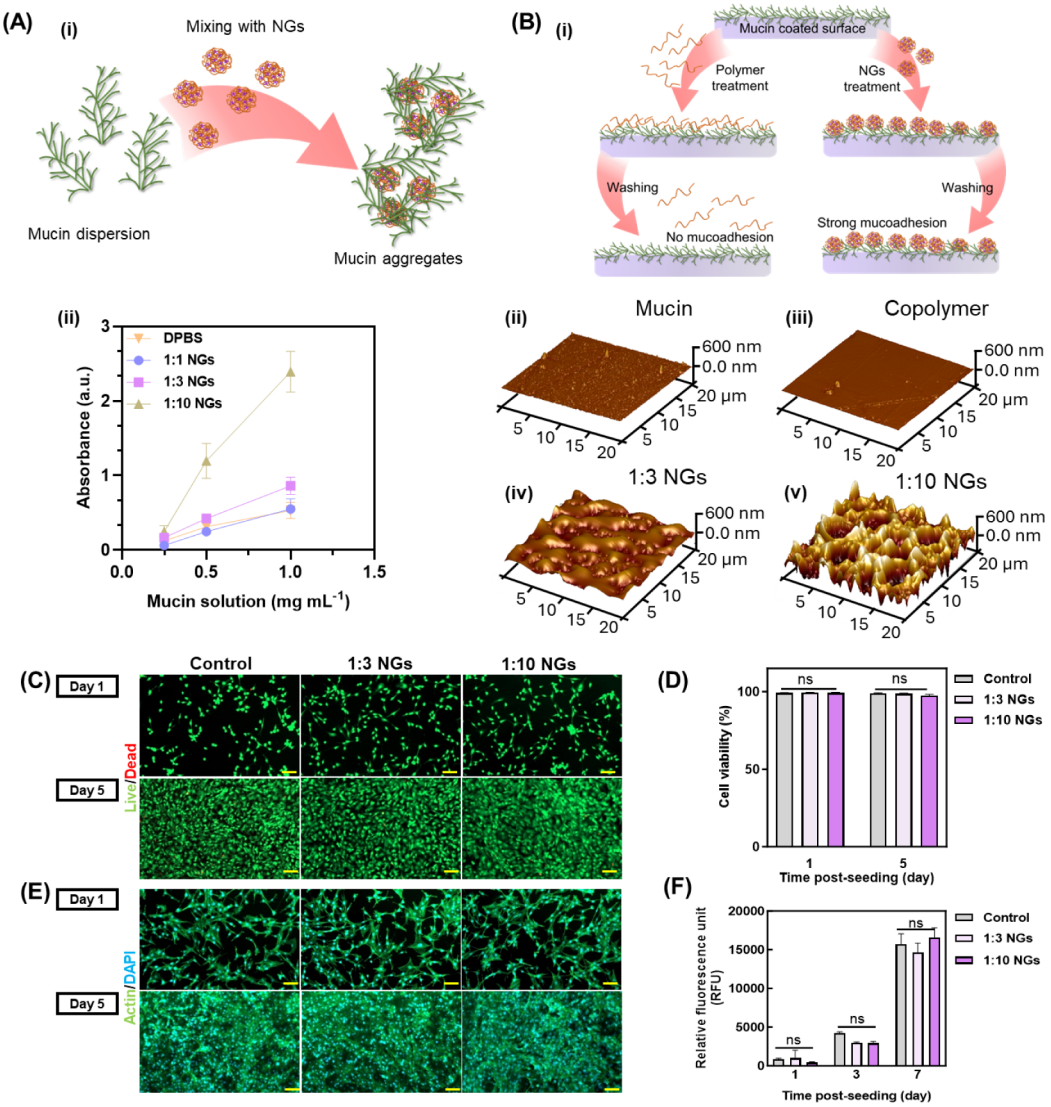

Figure 3. Evaluation of the mucoadhesion ability and *in vitro* biocompatibility of the NGs. (A) Schematic illustration of mucin-NGs aggregation leading to increased turbidity (i), and turbidity of mucin solutions at various concentrations mixed with NGs formed by using different copolymer/TA ratios (ii); (B) illustration of sample preparation for AFM assessment (i): AFM images of mucin-coated mica surfaces treated with DPBS (ii), copolymer (iii), the 1:3 NGs (iv), the 1:10 NGs (v); (C) representative Live/Dead images of 3T3 cells seeded on 48-well plates incubated with the NGs at 1 and 5 days postseeding (scale bars: 100 μm); (D) quantitative analysis of cellular viability at 1 and 5 days postseeding; (E) representative images of F-actin/DAPI stained 3T3 cells seeded on 48-well plates incubated with the NGs at 1 and 5 days postseeding (scale bars: 100 μm); (F) quantitative analysis of cellular metabolic activity using a PrestoBlue assay at 1, 3, and 7 days postseeding.

PEGMA) copolymer and NG solutions were measured using a Malvern Zetasizer. The copolymer exhibited a zeta potential of −18.6 ± 1.2 mV, attributed to carboxyl (CO−) groups at both ends of the copolymer chain, which originated from the chain transfer agent (CTA) used in polymerization (Figure 1I). The zeta potential of NGs with varying TA ratios became more negative compared to copolymer, ranging from −31.8 ± 1.6 mV to −49.3 ± 0.3 mV due to the acidic nature of the galloyl groups in TA (Figures 1I and S2B). This increase in zeta potential suggested the successful incorporation of TA into nanoaggregated copolymers.

TA incorporation into the nanoaggregated copolymers was further verified by UV−vis spectroscopy. The p(HexMA-PEGMA) copolymer showed an absorbance peak at 308 nm, attributed to the trithiocarbonate group at the end of polymer chain.[51] However, this peak was absent in the UV−vis spectra of the 1:10 NGs, where a new absorbance peak appeared at 277 nm, corresponding to TA (Figure 2A). The disappearance of the trithiocarbonate group's absorbance suggests that TA may have coated the surface of the NGs, in addition to cross-linking through H-bonding interactions. The formation of the NGs could also be monitored by performing a turbidity assay at a wavelength of 600 nm, where TA and the copolymer do not absorb light. As the ratio of TA increased, the turbidity of the NG solutions also increased, indicating the formation of a higher amount of stable NGs with increasing TA concentrations (Figure 2B). For example, NGs prepared with a 2:1 copolymer/TA ratio showed a transmittance value of 78.7 ± 1.7%, while transmittance decreased to 54.4 ± 1.7%, 20.3 ± 0.7%, 3.8 ± 0.1% and eventually zero for 1:1, 1:2, 1:3 and 1:10 copolymer/TA ratios, respectively (Figure 2C). This increase in turbidity indicates that higher TA concentrations led to a

https://doi.org/10.1021/acsnano.5c02002
ACS Nano 2025, 19, 27173−27191

greater yield of stable NGs formation. Conversely, with lower TA concentrations, the non-cross-linked copolymers were redissolved in water upon cooling the solution and removed during dialysis purification, resulting in a lower yield of NGs formation with lower turbidity. The amount of TA incorporated into NGs was determined utilizing a calibration curve of TA based on UV−vis absorbance values at 275 nm (Figure S3).

The TA content increased from 1.99 ± 0.01 mg at a copolymer/TA ratio of 2:1 to 5.81 ± 0.04 mg at a ratio of 1:10 when a fixed copolymer concentration of 5 mg/mL was used (Figure 2D). The H-bonding interactions between copolymer and TA were confirmed by Fourier transform infrared (FTIR) spectroscopy. The C═O stretching of TA exhibited a blue shift from 1702 cm^{-1} observed in TA spectra to 1719 cm^{-1} in TA-cross-linked NGs spectra, and the −OH stretching vibration shifted from 3355 cm^{-1} (in TA) to 3366 cm^{-1} (in TA-cross-linked NGs), indicating intermolecular H-bonding between the PEG repeating unit of the copolymer and TA (Figure 2E,F).[46,52] The NGs also displayed aliphatic C−H stretching peaks at 2873 and 2930 cm^{-1}, which were absent in the TA, as well as the aromatic C−O stretching vibrations at 1610 cm^{-1} that were not present in copolymer, confirming the successful incorporation of TA into the copolymer nanoaggregates (Figure 2F). As the TA ratio increased in the NGs, the intensity of the aliphatic CH_2 stretching peak decreased in the FTIR spectrum (Figure S4). These changes in FTIR peak intensities clearly indicated a higher amount of TA incorporated into the NG structure. To assess suitability of NGs for sustained therapeutic applications, we monitored the erosion (stability) of 1:10 NGs over a 14-day period at 37 °C by measuring their hydrodynamic sizes using DLS. The hydrodynamic size increased from 149.6 ± 2.0 nm on day 1 to 203.4 ± 1.2, 214.0 ± 1.2, 222.4 ± 1.2, 258.8 ± 2.0, and 307.7 ± 1.5 nm on days 3, 5, 7, 10, and 14, respectively (Figure S5A). The PDI of the NG solution remained below 0.1 throughout the first 10-day period, indicating good colloidal stability (Figure S5B). TA was incorporated into the NG network through noncovalent interactions with p(HexMA-PEGMA) copolymer, allowing its gradual release over time.[53] The observed increase in size is likely due to the release of TA, which led to swelling of the NGs as a result of reduced cross-linking density. This slow release is advantageous for maintaining ROS activity and achieving sustained therapeutic effects. Despite minor TA erosion over time, DLS data showed that the NGs maintained a consistent peak intensity distribution, further supporting their structural stability (Figure S5C).

Assessment of the Mucoadhesive Properties and *In Vitro* Biocompatibility of the NGs. Turbidity measurement is an *in vitro* method for qualitatively assessing the mucoadhesive properties of NPs.[54−56] We used this approach to evaluate the mucoadhesive properties of NGs with different copolymer/TA ratios. In this method, strong interactions between NGs and mucin led to the formation of randomly shaped microaggregates, resulting in increased turbidity (Figure 3A-i). The absorbance of different concentrations of mucin solutions mixed with NGs was recorded at 600 nm via UV−vis spectroscopy. Dulbecco's Phosphate Buffered Saline (DPBS) served as our control group. The 1:10 NGs exhibited the highest turbidity compared to the NGs with 2:1, 1:1, 1:2, 1:3, and 1:5 copolymer/TA ratios as well as DPBS, showing the importance of TA content for the mucoadhesive property of NGs (Figures 3A-ii and S6).

In addition to turbidity experiments, atomic force microscopy (AFM) was used to measure the interactions between mucoadhesive NGs and mucin. Mica surfaces were first spin-coated with mucin solution, followed by the addition of NGs, copolymer solution, or DPBS for 1 h. After washing the surfaces, AFM measurements were performed to assess surface roughness and height (Figure 3B-i). The roughness (Ra) of surfaces treated with DPBS and copolymer was around 8.11 and 3.63 nm, respectively (Figure 3B-ii, iii). The Ra of the mucin-coated mica surfaces treated with 1:3 NG was about 53.2 nm, but this value increased to around 181 nm for 1:10 NGs (Figure 3B-iv, v), confirming the adhesion and aggregation of the NGs onto the mucin surface. Based on AFM images, we also evaluated other roughness parameters, further confirming the mucoadhesiveness of the engineered NGs (Figure S7).

Topical eye drops remain the most common treatment for ocular diseases due to their ease of use and patient convenience. However, drug delivery through topical routes faces several structural and physiological barriers, such as the protective mucus membrane and tear production. The mucus membrane acts as a viscoelastic shield for the epithelial layer of ocular tissues, protecting them against foreign substances but also hindering drug penetration. Tear production, drainage, and corneal epithelium further limit drug absorption, decreasing the effectiveness of eye drop treatments for vision-threatening conditions. To address these challenges, the development of mucoadhesive drug delivery platforms is crucial for efficient ocular drug delivery. For instance, mucoadhesive drug-loaded NPs have been designed to prolong the residence time in the mucus membrane, thereby enhancing drug bioavailability, therapeutic efficacy and reducing the dosing frequency.[22] The mucoadhesive properties of a drug delivery system help extend its residence time on mucus surfaces by interacting with mucin glycoproteins. TA is known for its strong mucoadhesive characteristics, primarily due to the presence of gallol groups, which facilitate H-bonding interactions with the mucus layer.[26,27] Recent studies have also shown that TA can interact with the mucus layer via covalent interactions, specifically with thiol groups in the cysteine domains of mucin, resulting in even stronger mucoadhesion.[28] In our study, the turbidity and AFM results indicated that TA-cross-linked NGs have strong potential as effective mucoadhesive drug delivery vehicles for tissues with mucosal surfaces.

Next, we tested the *in vitro* cytocompatibility of engineered NGs using NIH 3T3 cells. Cells were seeded into well plates and exposed to NGs with copolymer/TA ratios of 1:3 and 1:10 to evaluate the effects of increasing TA content, while untreated cells served as the control group. The Live/Dead assay revealed excellent cellular viability (>95%) for both NGs and the control group over a period of 5 days postseeding (Figure 3C,D). Additionally, fluorescent staining of F-actin and cell nuclei verified the spreading and proliferation of cells exposed to the engineered NGs during the same time frame. As illustrated in Figure 3E, NGs supported cytoskeletal filament organization and spreading comparable to the untreated control group. Metabolic activity of the cells was also evaluated using the PrestoBlue assay, which measures the reduction of the reagent in the presence of metabolically active cells, producing a measurable fluorescent signal.[57] According to

https://doi.org/10.1021/acsnano.5c02002
ACS Nano 2025, 19, 27173−27191

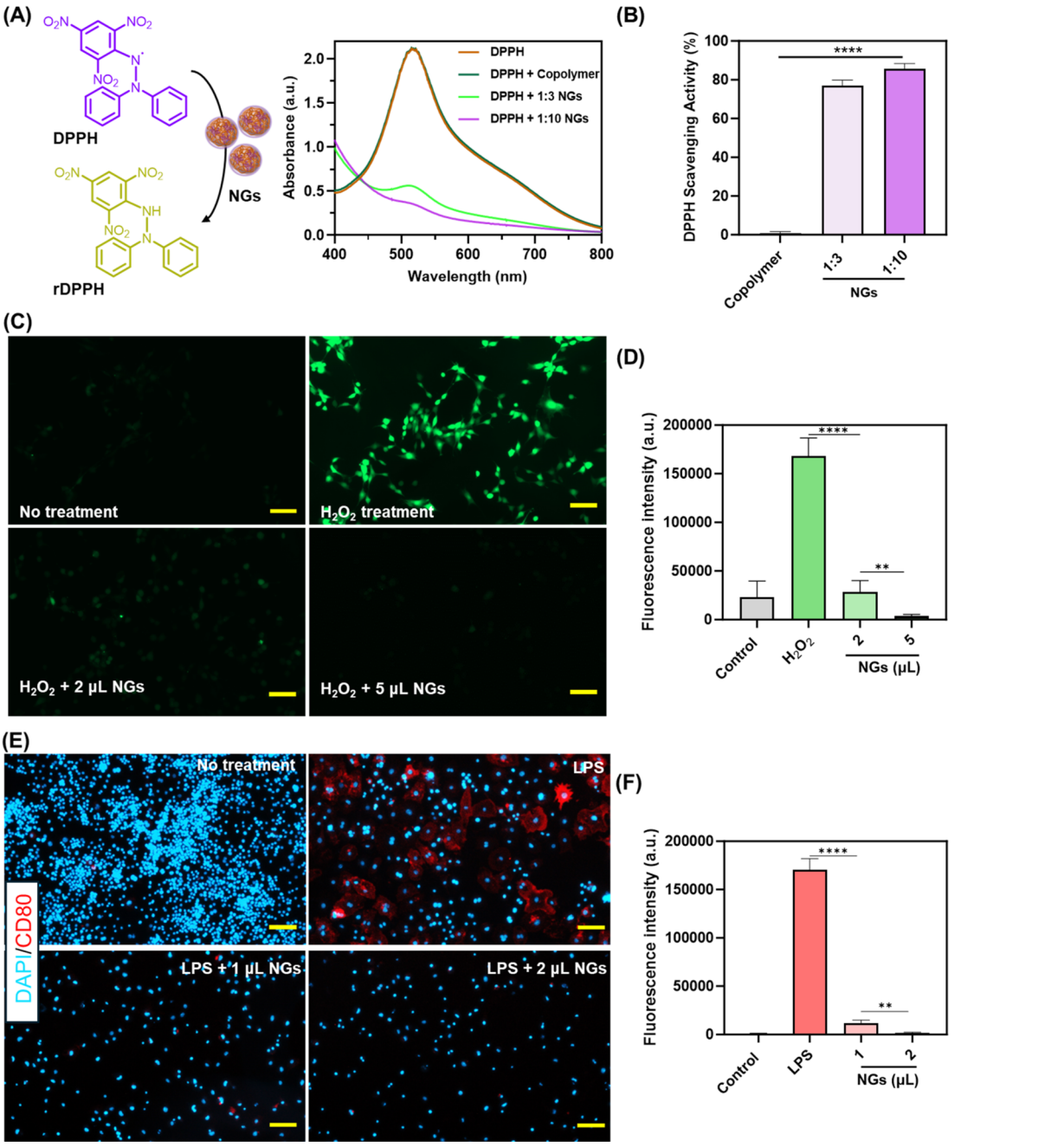

Figure 4. ***In vitro*** **ROS-scavenging and anti-inflammatory activity of NGs. (A) UV−vis absorbance of DPPH• solution before and after mixing with the copolymer and NGs formed at different copolymer/TA; (B) % DPPH• scavenging activities of NGs; (C) representative ROS stained (green fluorescence) images of 3T3 cells treated with H_2O_2 and H_2O_2 in combination with various concentrations of NGs, to assess intracellular ROS activity (scale bars: 100 μm); (D) quantitative analysis of DCFH-DA fluorescence intensity in 3T3 cells treated with H_2O_2, H_2O_2 + 2 μL NGs and H_2O_2 + 5 μL NGs in 300 μL culture media; (E) representative fluorescent microscopic images showing CD80 expression on macrophages. Macrophages were treated with LPS only, LPS with 1 μL NGs, LPS with 2 μL NGs, or left untreated (scale bars: 100 μm); (F) quantitative analysis of CD80 fluorescence intensity for macrophages under the same treatment conditions.**

Figure 3F, NIH 3T3 cells exposed to NGs at both ratios displayed steady proliferation over 7 days, with no significant differences relative to the control group. Overall, these findings confirmed the *in vitro* biocompatibility of the NGs, supporting their potential use for drug delivery applications.

In Vitro **ROS-Scavenging and Anti-Inflammatory Activity of Engineered NGs.** Free radicals on the ocular surface play a protective role in preventing oxidative damage to cells. However, excessive production of free radicals can overwhelm the eye's defenses, leading to oxidative stress. This imbalance may damage the cellular structures, resulting in inflammation, tissue degeneration, and potential vision problems.[58−60] TA, known for its strong radical-scavenging capacity due to its abundant hydroxyl groups, can be utilized as an antioxidant to treat ocular diseases associated with elevated ROS levels.[61,62] We evaluated the antioxidant activity of the engineered NGs against a stable free radical, 1,1-diphenyl-2-picrylhydrazine (DPPH•). Freshly prepared DPPH• solutions were mixed with the copolymer or NGs and incubated at room temperature for 5 min before UV−vis measurements. The

https://doi.org/10.1021/acsnano.5c02002
ACS Nano 2025, 19, 27173−27191

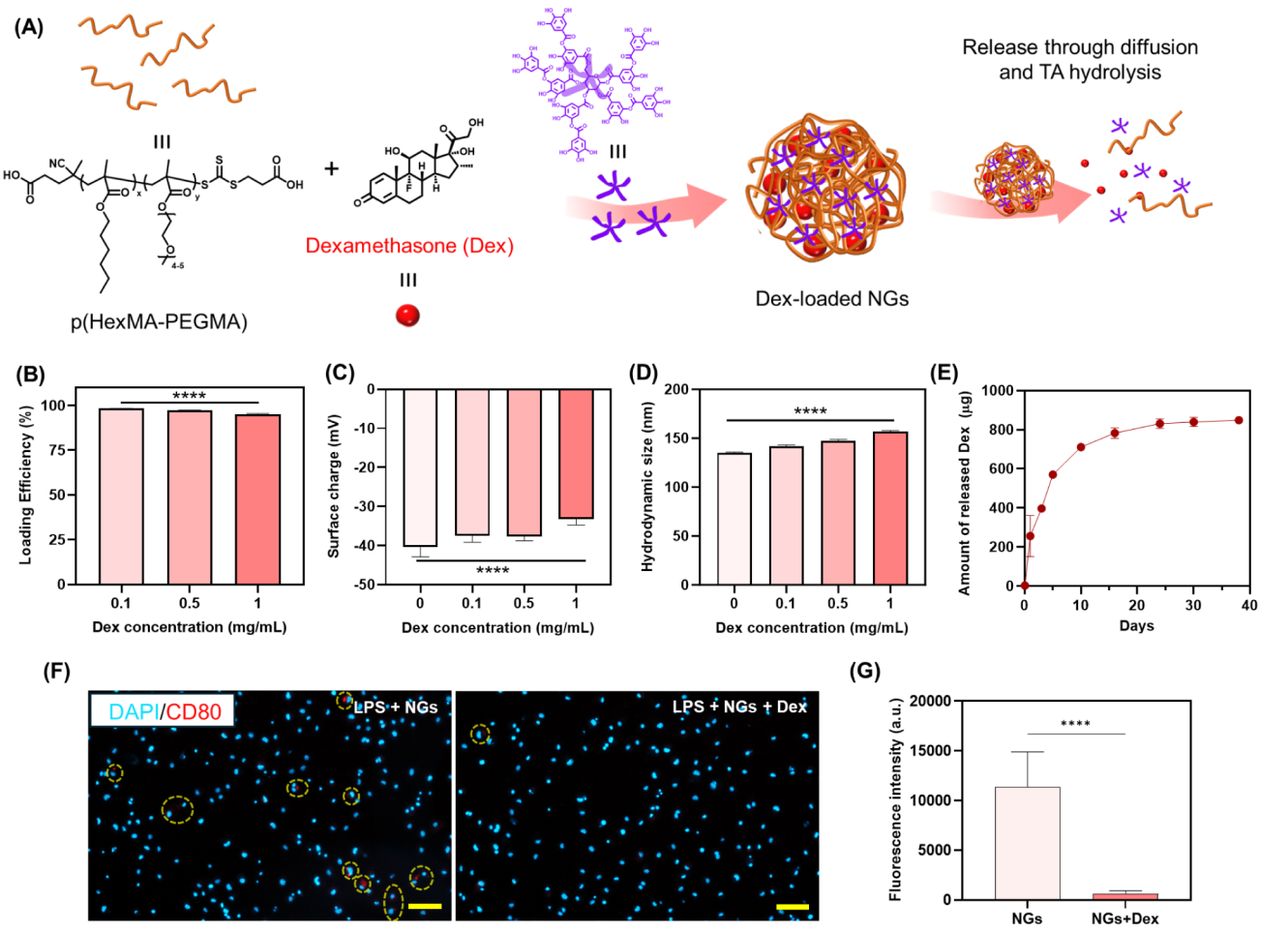

Figure 5. *In vitro* **drug loading, release profile and anti-inflammatory activity of the NGs. (A) Schematic illustration of Dex loading and release; (B) Dex loading efficiency; (C) zeta potential measurements and (D) hydrodynamic sizes of NGs containing varying drug concentrations; (E) drug release profile of Dex-loaded NGs (1 mg/mL); (F) representative fluorescent microscopic images showing CD80 expression on macrophages. Macrophages were treated with LPS with 1 μL NGs, LPS with 1 μL NGs loaded with Dex (scale bars: 100 μm); CD80 fluorescence signals are highlighted with yellow circles; (G) quantitative analysis of CD80 fluorescence intensity for macrophages under the same treatment conditions.**

absorbance peak at 517 nm, characteristic of DPPH•, decreased after mixing with NGs formed with varying copolymer/TA ratios (Figures 4A and S8A). The decrease in UV absorbance of DPPH• confirmed that the NGs exhibited high radical scavenging activity. However, no change in absorbance was observed when the copolymer was added to the DPPH• solution, indicating that the p(HexMA-PEGMA) copolymer lacked antioxidant activity. We also calculated the percentage of DPPH• scavenging activity for both NGs and the copolymer. The 1:3 NGs exhibited 77.0 ± 2.2% scavenging activity, while the 1:10 NGs achieved 85.6 ± 2.0% after mixing with DPPH• solution for 5 min. In contrast, the copolymer showed no scavenging activity, as no change in UV absorbance was observed during the test (Figure 4B). Moreover, the 2:1 NGs, with the lowest TA ratio, showed 51.6 ± 1.4% scavenging activity, while the other NGs formulations demonstrated over 75% activity, reaching up to 85.6 ± 2.0% for the 1:10 NGs (Figure S8B).

The ROS scavenging activity of NGs was further investigated *in vitro* using the 2′,7′-dichlorofluorescin diacetate (DCFH-DA) assay. In this assay, the intracellular ROS levels were indicated by a green fluorescent signal.[63−65] Cells treated with hydrogen peroxide (H_2O_2) exhibited a marked increase in fluorescence, reflecting elevated ROS levels. However, when NGs were introduced at 2 and 5 μL in 300 μL culture media, a significant reduction in fluorescence intensity was observed, with stronger ROS scavenging effects at the higher NG concentration (Figure 4C,D). The ROS-scavenging efficacy of the NGs could be attributed to the presence of the TA molecule in the NG structure.

The anti-inflammatory activity of the engineered NGs was also evaluated *in vitro* using RAW 264.7 macrophage cells activated by LPS, a known stimulant that interacts with macrophages primarily via Toll-like receptor 4 (TLR4), initiating a strong immune response. After activation with LPS, the RAW 264.7 cells were treated with two concentrations of NG solutions (1 and 2 μL in 300 μL culture media). Fluorescent microscopy revealed that the NGs significantly reduced the expression of the cluster of differentiation 80 (CD80), a marker associated with activated macrophages, compared to the LPS-treated cells without NGs (Figure 4E). In cells not treated with NGs, LPS activation resulted in a pronounced increase in CD80 red fluorescence intensity, indicating enhanced inflammatory activity (Figure 4E,F). These findings suggest that the anti-inflammatory effects of the NGs may be attributed to the TA groups within their

https://doi.org/10.1021/acsnano.5c02002
ACS Nano 2025, 19, 27173−27191

structure, which are known for their anti-inflammatory properties.[66]

Drug Loading/Release Studies, Shear-Thinning Behavior, and Anti-Inflammatory Activity of the Drug-Loaded NGs. Delivering hydrophobic drugs to ocular tissues is challenging due to their poor solubility and difficulty in penetrating ocular barriers. Many ocular drugs, including corticosteroids like Dex, antiglaucoma drugs like latanoprost, and nonsteroidal anti-inflammatory drugs (NSAIDs) like ketorolac, are hydrophobic,[67,68] which limits their effectiveness through rapid clearance and low retention. Our TA-cross-linked NG platform improves the penetration of these hydrophobic drugs by facilitating their solubilization and enhancing their ability to cross ocular barriers. By encapsulating hydrophobic compounds and providing sustained release, the NGs increase the efficiency of drug delivery, improving retention and therapeutic outcomes for ocular diseases that require hydrophobic agents. The p(HexMA-PEGMA) copolymer consists of hydrophobic hexyl units and hydrophilic PEG side groups within the polymer chain. This combination allows the copolymer to self-assemble into nanoaggregates upon heating, which serves as versatile drug delivery vehicles after TA cross-linking. The engineered NGs are capable of delivering hydrophobic drugs within their three-dimensional cross-linked network, thanks to the presence of hydrophobic hexyl units in the polymer chain. In this study, we utilized these hydrophobic groups to load Dex, as a model hydrophobic drug, within the NGs network (Figure 5A). In addition to hydrophobic interactions, H-bonding can also contribute to the drug loading process, as Dex contains three hydroxyl (−OH) groups that can form hydrogen bonds with PEG groups in the NGs. This combination of hydrophobic and H-bonding interactions is expected to enhance the encapsulation and retention of Dex within the NGs. We investigated the Dex loading capacity of the NGs using different concentrations of Dex. It was found that drug concentration did not affect the loading capacity, as it remained nearly 100% for all drug concentrations tested (Figure 5B). The zeta potential of the NGs after Dex loading showed a slight increase, ranging from −40.8 ± 1.8 mV to −33.5 ± 1.1 mV (Figure 5C). Moreover, increasing the amount of Dex loaded into the NGs did not significantly impact their hydrodynamic sizes, with only a slight increase observed at higher drug concentrations (Figure 5D). All Dex-loaded NGs exhibited very low PDI values, remaining below 0.1, indicating that drug loading has no negative effect on size distribution (Figure S9). After characterizing the Dex-loaded NGs, we conducted a drug release study to evaluate the release profile of NGs loaded with 0.857 mg of Dex. The release experiment was performed in DPBS at 37 °C over a period of 38 days. The NGs exhibited a sustained release of Dex, gradually releasing their payload with a 96.99 ± 2.79% cumulative release within the first 24 days (Figures 5E and S10). The release of hydrophobic Dex occurred primarily through a diffusion process, facilitated by the nanopores on the NG structure. On the other hand, the gradual degradation of TA through hydrolysis contributed to the controlled release of Dex from the NG network, making them ideal for sustained drug delivery.[69,70] This sustained release profile suggested that the NGs could be an effective drug delivery system for prolonged therapeutic application on the eye, reducing the need for frequent dosing and improving patient compliance.

To assess the rheological properties of the NG formulations, we conducted shear rate−dependent viscosity measurements at physiologically relevant temperature to characterize their shear-thinning behavior, an essential feature for ocular drug delivery. Shear-thinning enables the formulation to flow under stress, such as during blinking, while recovering viscosity once the stress is removed, thereby enhancing retention on the ocular surface. Importantly, the developed NGs remained in a liquid-like state at ocular surface temperature (~35 °C), as confirmed by rheological measurements showing low viscosity and shear-thinning behavior across physiologically relevant shear rates. Both blank and Dex-loaded NG formulations showed shear-thinning properties, attributed to dynamic/reversible H-bonding between TA and p(HexMA-PEGMA) copolymer (Figure S11A).[71] These interactions break under shear and reform when the shear is removed. At a shear rate of 1000 s^{-1}, close to the rate experienced during blinking, both NGs and Dex-loaded NGs had a viscosity of approximately 10 mPa s (Figure S11B).[72] This viscosity range (10−30 mPa s) is within the range reported for commercially available eye drop formulations, which are designed to minimize discomfort and avoid excessive stickiness during blinking.[73]

The anti-inflammatory activity of Dex-loaded NGs was also evaluated *in vitro* using RAW 264.7 macrophage cells. After activation with LPS, these cells were treated with Dex-loaded NGs (1 μL in 300 μL culture media), while NGs without Dex at the same concentration served as the control group. Dex-loaded NGs reduced CD80 expression compared to unloaded NGs (Figure 5G), as evidenced by higher red fluorescence intensity in cells treated with unloaded NGs than in those treated with Dex-loaded NGs (Figure 5F), indicating decreased inflammatory activity in the presence of Dex. Both NGs and Dex-loaded NGs suppressed CD80 expression relative to the LPS-treated group, with discernible differences primarily observed at lower concentrations. At low doses (*e.g.,* 1 μL), Dex-loaded NGs achieved greater suppression of inflammation than NGs alone. However, at higher concentrations (*e.g.,* 2 μL), NGs alone were sufficient to suppress inflammation to levels comparable to those achieved by Dex-loaded NGs (Figure 4F), resulting in minimal differential effect. This outcome may be attributed to the short duration of this *in vitro* model (48 h), during which the intrinsic ROS-scavenging and anti-inflammatory properties of the NGs likely provided adequate suppression of acute inflammatory responses, potentially masking any additional benefit from Dex.

Dex is a clinically approved corticosteroid broadly used to treat severe and complex inflammatory diseases, including ocular conditions.[74] While the TA groups within the NGs confer inherent antioxidant and anti-inflammatory properties, they lack the extensive clinical validation required for the treatment of ocular inflammation.[75] TA primarily exerts its anti-inflammatory effect by scavenging ROS and inhibiting specific pro-inflammatory enzymes.[76] However, this antioxidant-based mechanism may be insufficient for addressing more severe or chronic inflammatory conditions. Therefore, the incorporation of Dex into the NGs is critical to enhance their therapeutic potency, particularly for the treatment of complex or persistent inflammation where TA alone may not provide sufficient efficacy.

To test the efficacy of our engineered NGs for loading hydrophilic drugs, we used moxifloxacin (MFX), a commonly used antimicrobial agent for treating various types of infections, as a model hydrophilic drug (Figure S12A). The loading of MFX into the NG network was primarily driven by electrostatic interactions, as the engineered NGs were

https://doi.org/10.1021/acsnano.5c02002
ACS Nano 2025, 19, 27173−27191

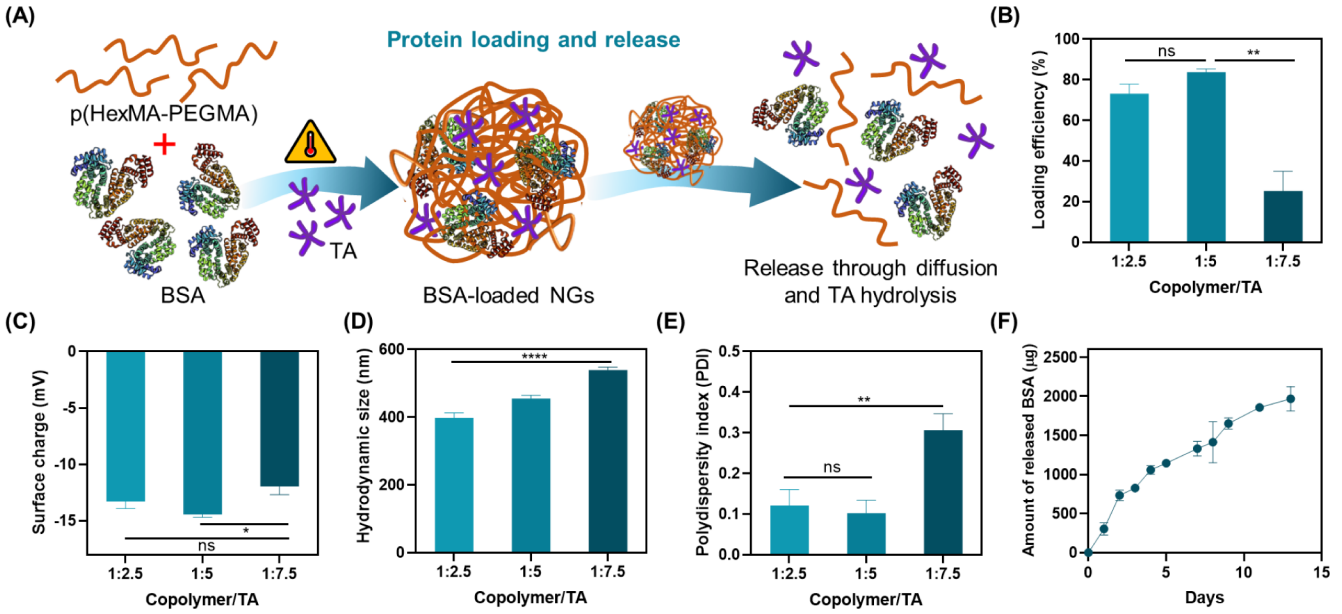

Figure 6. *In vitro* BSA loading into the NGs. (A) Schematic illustration of BSA loading and release; (B) BSA loading efficiency; (C) zeta potential measurements; (D) hydrodynamic sizes; (E) PDIs; (F) drug release profile of BSA-loaded NGs.

negatively charged, while MFX is a positively charged molecule. Additionally, the hydrophilic PEG network within the NGs further facilitated the encapsulation of MFX. We investigated the MFX loading efficiency of the NGs across various MFX concentrations. The loading efficiency was approximately 80% for MFX concentrations of 0.5%, 0.8%, 1.2% and 1.5%. However, a decreased loading efficiency to 59.3 ± 0.2% was observed at an MFX concentration of 2%, likely due to saturation of the NGs (Figure S12B). The concentrations of MFX loaded into NGs were higher than those in commercially available MFX eye drops (0.5% solution = 5 mg/mL) for all groups, except for the loading experiment conducted with 0.5% MFX, where the drug content was 4.3 mg/mL. The zeta potential of the NGs shifted from negative to positive after loading MFX, indicating that the drug molecules electrostatically interacted with the negatively charged NGs (Figure S12C). Additionally, the hydrodynamic size of the NGs slightly increased after MFX loading, while the PDI remained below 0.1 for all samples prepared with different MFX concentrations, showing no significant change (Figure S12D,E). In conclusion, the hydrophilic PEG network within the NGs facilitated the encapsulation of hydrophilic drug molecules by providing a water-compatible environment. Simultaneously, the hydrophobic hexyl side groups created domains within the NGs that could interact with and encapsulate hydrophobic drug molecules. This dual functionality makes the engineered NGs highly adaptable for delivering a broad range of therapeutic agents. Additionally, these TA-cross-linked mucoadhesive NGs provide stability with their cross-linked structure. TA-cross-linked NGs also outperform conventional eye drops by maintaining higher drug bioavailability, avoiding rapid clearance from the eye due to mucoadhesion, and reducing the need for frequent administration.

Protein Loading into NGs and the Release Study. Protein delivery is crucial in ocular drug delivery as proteins, including antibodies, enzymes, and growth factors, play key roles in treating various ocular diseases, such as age-related macular degeneration (AMD), diabetic retinopathy, and ocular infections.[77−79] Proteins often offer targeted therapeutic effects that small-molecule drugs cannot achieve, such as promoting tissue regeneration, modulating immune responses, or inhibiting specific disease pathways.[80−82] However, their large size, instability, and poor ability to cross ocular barriers make their delivery to the eye a significant challenge. Our NG platform can potentially address these issues by encapsulating proteins in a protective matrix that enhances their stability and prevents degradation. The NGs' ability to self-assemble and provide sustained release ensures controlled delivery of proteins, improving their retention on the ocular surface and enhancing their therapeutic efficacy. This capability offers a promising solution for overcoming the barriers to protein delivery in ocular therapies. As a proof of concept, we investigated bovine serum albumin (BSA) loading in the engineered NGs (Figure 6A). To avoid large aggregate formation, we tested various copolymer/TA ratios (1:2.5, 1:5, and 1:7.5) to determine an optimal balance between high loading efficiency and tissue penetration. The highest loading efficiency, 83.8 ± 2.7%, was achieved at a 1:5 copolymer/TA ratio (Figure 6B). After BSA loading, the zeta potential of the NGs increased and remained in the range of −12 ± 1.7 mV to −13.3 ± 1.5 mV (Figure 6C). The hydrodynamic size of the BSA encapsulated NGs also increased significantly, while the PDI remained below 0.3 for all NGs formed at varying copolymer/TA ratios (Figure 6D,E). The NGs exhibited sustained release of BSA, with approximately 94.8 ± 7.5% cumulative release within the first 14 days (Figures 6F and S13). This release profile suggests that NGs may serve as a delivery system for large biomolecules in prolonged ocular disease treatment, with the potential to reduce dosing frequency and improve patient compliance. Many eye diseases rely on protein-based therapeutics, which benefit from a sustained release profile.[77] For example, AMD and diabetic retinopathy require antivascular endothelial growth factor (anti-VEGF) proteins to manage retinal damage and vascular complications.[83] Our mucoadhesive NGs enable extended release, minimizing the need for frequent, invasive intravitreal injections. In conditions like dry eye syndrome, corneal

https://doi.org/10.1021/acsnano.5c02002
ACS Nano 2025, 19, 27173−27191

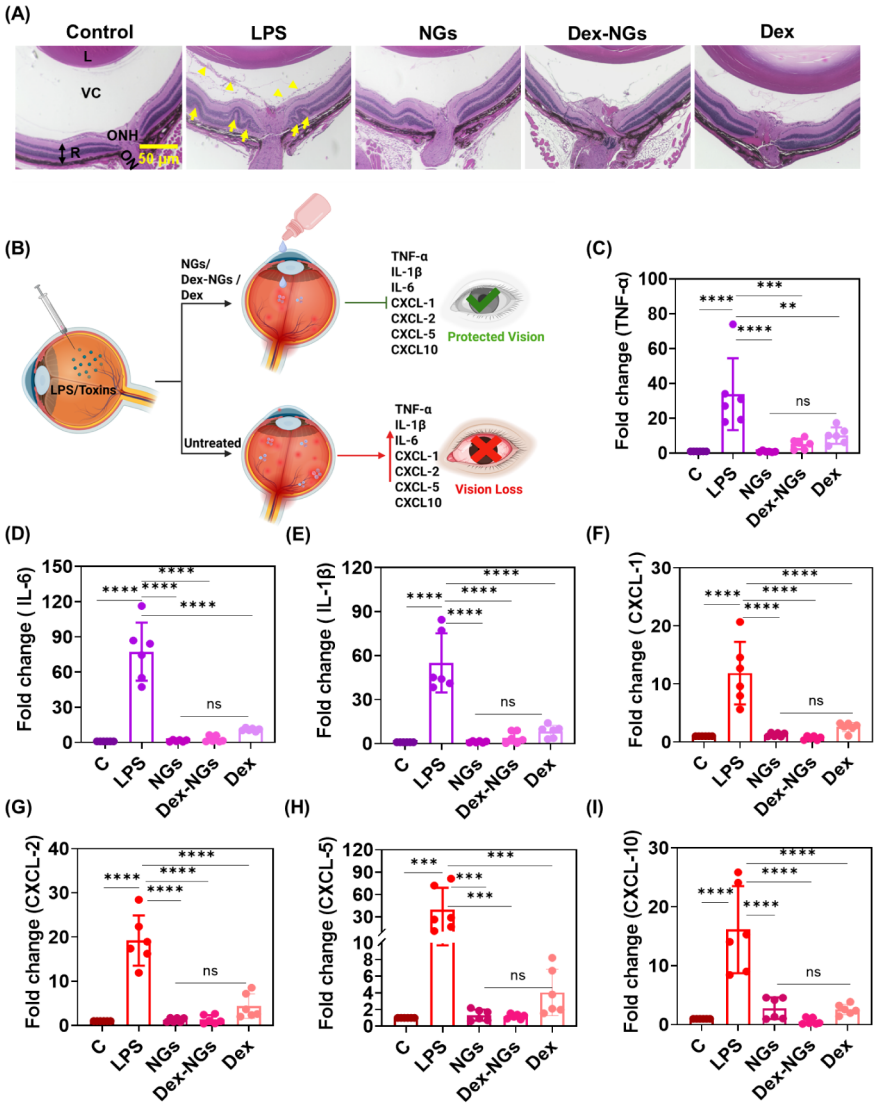

Figure 7. Therapeutic efficacy of blank NGs and Dex-loaded NGs in a mouse model of intraocular inflammation. (A) Representative H&E-stained images of retinal tissues 48 h post-treatment. Both blank NGs- and Dex-loaded NGs and Dex-treated eyes showed intact tissue architecture and reduced cellular and fibrin infiltrates, which are comparable to healthy controls, indicating no observable toxicity by NGs and a protective response. In contrast, LPS-treated eyes exhibited retinal folds/detachments, along with heavy fibrin and immune cell infiltration (highlighted with yellow arrows), indicating intraocular inflammation and inflammation-induced retinal damage. (L: Lens, VC: Vitreous Chamber, ONH: Optic Nerve Head, ON: Optic Nerve, R: Retina); (B) schematic depicting the model of intraocular inflammation resulting in vision loss and blank NGs/Dex-NGs/Dex treatment leads to protected vision. C57BL/6 WT (n = 6/group) were intravitreally injected with LPS and treated topically with blank NGs, Dex-loaded NGs (Dex-NGs) or Dex solution (free drug). At 48 h post-treatment, retinal tissue was harvested and subjected to ribonucleic acid (RNA) extraction and qRT-PCR for (C) TNF-α; (D) IL-6; (E) IL-1β; (F) CXCL-1; (G) CXCL-2; (H) CXCL-5; (I) CXCL-10. The schematic diagram was created using BioRender software (biorender.com).

injuries, and uveitis, proteins such as growth factors, cytokines, and anti-inflammatory biologics are essential for healing and inflammation control.[84,85] NGs facilitate localized, controlled delivery, enhancing therapeutic outcomes while reducing the burden of frequent administration. By addressing these critical needs, the engineered NGs present a transformative solution for improving efficacy and patient adherence in treating a wide range of ocular diseases.

***In Vivo* Biocompatibility and Therapeutic Efficacy of NGs and Dex-Loaded NGs in a Mouse Model of Intraocular Inflammation.** We first assessed NGs' ocular biocompatibility using hematoxylin and eosin (H&E) staining before evaluating the therapeutic efficacy of the NGs. Histological analysis of retinal tissues 48 h after topical application of blank NGs and Dex-loaded NGs revealed no signs of structural disruption, immune cell infiltration, or tissue damage compared to untreated controls (Figure 7A), indicating excellent biocompatibility. In contrast, the LPS-treated group exhibited marked retinal folding/detachments, fibrin and immune cell infiltration, and disruption of retinal architecture, confirming successful induction of intraocular inflammation and inflammation-mediated damage (Figure 7A, marked with yellow arrows). These findings validate both the safety of the NG formulation and the effectiveness of the inflammation model for subsequent therapeutic evaluation.

To test the therapeutic efficacy of blank NGs and drug-loaded NGs, we use a corticosteroid, Dex, as a candidate drug widely used in human and veterinary ophthalmology

https://doi.org/10.1021/acsnano.5c02002
ACS Nano 2025, 19, 27173−27191

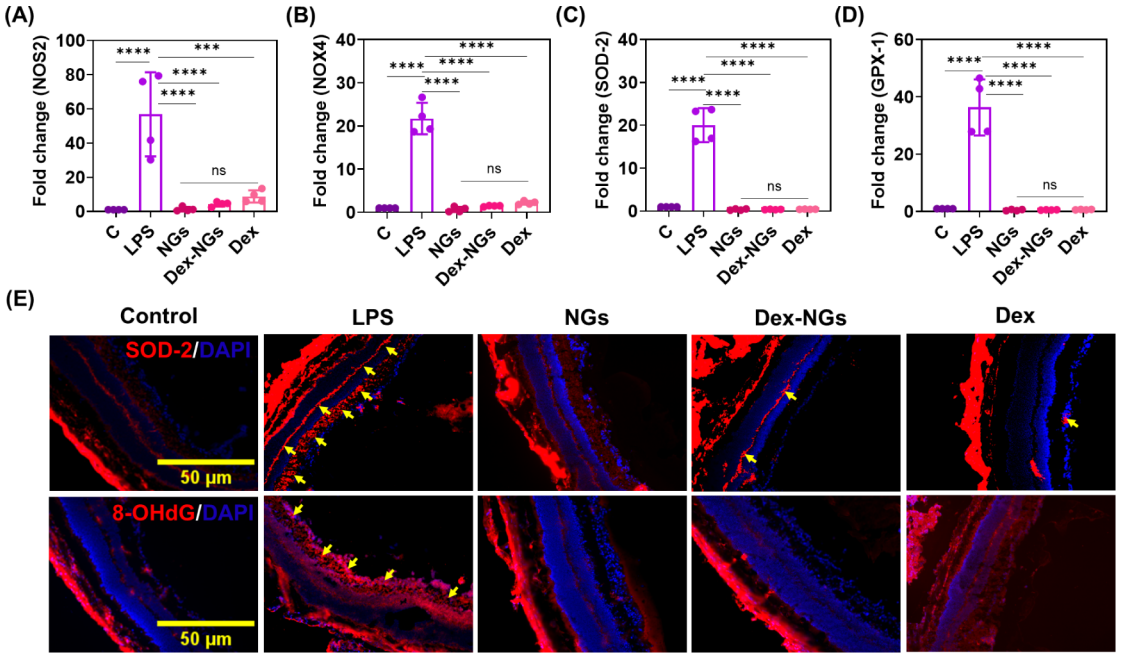

Figure 8. ***In vivo*** **evaluation of ROS scavenging activity of NGs and Dex-loaded NGs in a mouse model of intraocular inflammation. (A–D) Quantitative PCR analysis of retinal tissue 48 h post-treatment showing relative mRNA expression levels of oxidative stress–related enzymes: inducible NOS2, NOX4, SOD-2, and GPX-1. Treatment with blank NGs, Dex-loaded NGs, or free Dex significantly reduced NOS2, NOX4, SOD-2, and GPX-1 expression compared to the LPS-treated group. (E) Representative immunofluorescence images of retinal cryosections immunostained for SOD-2 and 8-OHdG. All treatment groups showed decreased SOD-2 expression and reduced 8-OHdG accumulation compared to LPS-only controls (a few representative cells are marked with yellow arrows), confirming ROS scavenging at the tissue level, n = 4.**

applications to treat intraocular inflammation.[86,87] Intraocular inflammation was induced by a single intravitreal injection of LPS (100 ng/eye) (Figure 7B). NGs or Dex-loaded NGs were applied topically twice a day, 6 h post-LPS injection. The pure Dex (free drug) ophthalmic solution was used as a control drug. The neural retina was harvested 48 h after treatment, and levels of inflammatory cytokines were quantified using real-time polymerase chain reaction (qPCR). Our qPCR analysis revealed a significant reduction in LPS-induced proinflammatory mediators such as tumor necrosis factor alpha (TNF-α), interleukin-1 beta (IL-1β), IL-6, C-X-C motif chemokine ligand 1 (CXCL-1), and CXCL-10, in both the blank NGs and Dex-loaded NGs groups, which were all comparable to free drugs (Figure 7C–I). These results demonstrate that blank NGs alone can suppress intraocular inflammation, suggesting they possess intrinsic anti-inflammatory activity.

Given the eye's immune-privileged status, even localized inflammation can result in irreversible damage and vision loss. Bacterial cell wall components such as LPS, peptidoglycan, and lipoteichoic acid have been shown to induce intraocular inflammation and degeneration.[88−90] While current therapeutic approaches, such as topical eye drops, and periocular or intraocular injections, remain standard,[91] they are often limited by poor retention, rapid clearance, and restricted drug bioavailability. Nanoparticle-based systems have improved some aspects of ocular delivery, yet most function solely as passive carriers without therapeutic activity. In contrast, our TA-cross-linked NGs offer a distinct advantage by combining efficient drug encapsulation and a sustained release proflie with native anti-inflammatory and ROS-scavenging properties. This dual functionality enables the NGs to act not only as delivery vehicles but also as active agents capable of suppressing inflammation in the absence of loaded drugs. This feature is particularly advantageous for the treatment of acute or moderate ocular inflammation, where a steroid-free platform may be desirable to minimize side effects or extend therapeutic utility.

Although blank NGs were effective in suppressing acute inflammation, the incorporation of Dex remains important for managing more severe or chronic conditions. As the current model captures only short-term responses, future studies will focus on long-term or recurrent intraocular inflammation models to fully evaluate the added benefit of Dex and the therapeutic impact of sustained drug release. Specifically, we aim to determine whether a single application of Dex-loaded NGs can maintain anti-inflammatory efficacy over time, potentially reducing the need for repeated dosing compared to free drugs. In addition, future studies are required to test the suitability of NGs as vehicles in other chronic ocular diseases such as glaucoma.

A key advantage of our NG platform lies in its ability to codeliver diverse therapeutics. This unique feature will be explored in future studies to enable combined therapy, such as the codelivery of Dex and anti-VEGF agents, for treating neovascularization and scarring/fibrosis in ocular injuries. These conditions require complex regimens involving both anti-inflammatory and antiangiogenic drugs, which often challenge patient compliance and affect visual outcomes. The ability of our NGs to simultaneously deliver these therapeutics offers a novel approach to simplifying treatment and improving efficacy for patients with complex ocular diseases.

In Vivo **ROS Scavenging of NGs and Dex-Loaded NGs in a Mouse Model of Intraocular Inflammation.** To further elucidate the mechanism behind the observed anti-

https://doi.org/10.1021/acsnano.5c02002
ACS Nano 2025, 19, 27173−27191

inflammatory effects, we evaluated oxidative stress markers at the tissue level in the same LPS-induced intraocular inflammation model. qPCR analysis of neural retinal tissue revealed that treatment with blank NGs, Dex-loaded NGs, and free Dex significantly downregulated the expression of inducible nitric oxide synthase (NOS2) and NADPH oxidase 4 (NOX4) (Figure 8A,B), the two key enzymes involved in the generation of ROS.[92] Interestingly, the expression of antioxidant enzymes superoxide dismutase 2 (SOD-2) and glutathione peroxidase 1 (GPX-1) was also reduced following treatment (Figure 8C,D). This downregulation likely reflects a diminished oxidative burden,[93] as reduced ROS levels lessen the compensatory upregulation of endogenous antioxidant defenses.

To further confirm the ROS scavenging activity in our treatment groups, we performed immunofluorescence staining on retinal cryosection for superoxide dismutase (SOD-2) and 8-hydroxy-2′-deoxyguanosine (8-OHdG), a well-established marker of oxidative DNA damage.[94] Our results revealed that NGs, Dex-loaded NGs, and free Dex-treated eyes drastically reduced the LPS-induced expression of SOD-2 and 8-OHdG, in comparison to LPS-injected and untreated mice (Figure 8E). This direct evidence of ROS scavenging in ocular tissue confirms that the NGs exert antioxidant effects locally within inflamed retinal environments.

Importantly, there were no statistically significant differences among the NGs, Dex-NGs, and Dex groups across all assessed oxidative stress markers, strongly supporting that the blank NGs possess potent ROS-scavenging activity *in vivo*. These findings help to explain the comparable anti-inflammatory efficacy observed across treatment groups and validate the NGs as an intrinsically bioactive therapeutic platform. Clinically, this intrinsic ROS-scavenging function enables the NGs to serve not only as a delivery vehicle but also as standalone therapeutics, particularly valuable for steroid-sparing strategies in ocular inflammation. Their biocompatibility, mucoadhesive properties, and capacity for sustained drug release further enhance their potential as a noninvasive, patient-friendly treatment for ocular diseases driven by oxidative stress and inflammation.

STUDY LIMITATIONS

Although the synthesis of mucoadhesive NGs is relatively straightforward, typically involving one-step copolymerization of commercially available monomers followed by TA cross-linking, scaling up the process requires careful reoptimization. This system is sensitive to formulation parameters, and simply increasing TA proportionally based on a small-scale protocol often results in NG aggregation and loss of size uniformity. This suggests that TA-induced cross-linking does not scale linearly with reaction volume or copolymer concentration, necessitating tailored adjustments to maintain colloidal stability. While large-scale production is feasible, it requires fine-tuning of copolymer and TA concentrations, as well as close control over mixing conditions to ensure consistent quality. In some cases, advanced fabrication techniques such as microfluidic-assisted synthesis may help improve reproducibility and process control during scale-up.[12,95] Another limitation worth noting is that the engineered mucoadhesive NGs may cause temporary blurred vision upon ocular application due to their inherently milky appearance. However, this is a common and generally temporary effect observed in many NP-based formulations and steroid-containing eye drops. In addition, while strong mucoadhesion typically limits NP diffusion toward epithelial cells and reduces the likelihood of cellular uptake, this effect is not absolute. The extent of cellular interactions depends on multiple factors, including mucin layer integrity, exposure time, and NP properties. Our system was designed to promote surface retention via TA-mediated mucoadhesion, which is expected to reduce rapid cellular internalization. However, we acknowledge that direct evidence of the interaction sequence (mucin binding vs cellular uptake) was not assessed in this study and further investigation is needed.

CONCLUSIONS

In this study, we successfully developed self-assembled NGs cross-linked with antioxidant and mucoadhesive TA, leveraging H-bonding interactions. This straightforward approach allowed us to design a versatile drug delivery platform capable of encapsulating hydrophilic, hydrophobic drugs and large protein molecules. The engineered NGs exhibited excellent mucoadhesion, antioxidant, and anti-inflammatory properties *in vitro*, along with high cytocompatibility. The NGs demonstrated significant potential for the treatment of intraocular inflammation in preclinical mouse models. Furthermore, this concept can be readily adapted for targeted drug delivery to other mucus-coated regions of the body, such as vaginal, intestinal, lung, and nasal areas, making it a promising platform for a wide range of therapeutic applications.

EXPERIMENTAL SECTION

Materials. 4-((((2-Carboxyethyl)thio)carbonothioyl)thio)-4-cyanopentanoic acid, AIBN, TA, porcine gastric mucin, DCFH-DA, MFX hydrochloride and LPS (L4391) were purchased from Sigma-Aldrich (St. Louis, MO), and used without further purification. HexMA and PEGMA (M_n = 300) monomers were purchased from Sigma-Aldrich and purified over neutral aluminum oxide before use. Dex was obtained from TCI Chemicals. All other organic solvents were purchased from Thermo Fisher Scientific. Dulbecco's modified Eagle medium (DMEM) was purchased from Cellgro (Manassas, VA). Fetal Bovine Serum (FBS) and DPBS were obtained from HyClone (Logan, UT). Penicillin/streptomycin (Pen-Strep), a Live/Dead viability kit, LPS, Anti-CD80 antibody were purchased from Invitrogen, Thermo Fisher Scientific. H_2O_2 was purchased from Fisher Chemicals. The qRT-PCR gene-specific primers for the pro-inflammatory cytokines (TNFα, IL-1β, IL-6) and chemokines (CXCL-1, CXCL-2, CXCL-5, CXCL-10) were synthesized from Integrated DNA Technologies (Coralville, IA)

METHODS

Synthesis of p(HexMA-PEGMA) Copolymer. HexMA (237.16 mg, 1.39 mmol), PEGMA (978.15 mg, 3.26 mmol), CTA (20 mg, 0.065 mmol), and AIBN (0.53 mg, 3.3 μmol) were dissolved in 2.4 mL of dimethylformamide (DMF). The reaction mixture was purged with nitrogen (N_2) for 30 min and then immersed in a preheated oil bath at 65 °C for 16 h. The reaction was terminated by exposing it to air and allowing the temperature to cool to 25 °C in an ice bath. The solvent was removed by rotary evaporation, and the resulting p(HexMA-PEGMA) copolymer was precipitated in cold diethyl ether (Et_2O). The copolymer was collected and dried under a vacuum overnight (1.05 g, 85% yield). The molar mass and dispersity ($Đ$) of p(HexMA-PEGMA) were determined by SEC analysis. $M_{n,theo}$ = 16 100 g/mol, $M_{n,SEC}$ = 17 300 g/mol, M_w/M_n = 1.25.

LCST Measurements of p(HexMA-PEGMA) Copolymer. The copolymer was dissolved in water at a concentration of 5 mg/mL. The LCST of the copolymer was determined by measuring absorbance values at 600 nm across different temperatures using UV−vis

https://doi.org/10.1021/acsnano.5c02002
ACS Nano 2025, 19, 27173−27191

spectroscopy. % transmittance was calculated using eq 1 and plotted against temperature. The size of the nanoaggregates at 25 °C and above the LCST was measured by DLS.

$$\% T = 10^{2-A} \quad (1)$$

^{1}H NMR Characterization of the p(HexMA-PEGMA) Copolymer. The copolymer was characterized by ^{1}H NMR spectroscopy using a 400 MHz Bruker AV400 spectrometer (32 scans, 2-s delay). The spectra were recorded at 25 °C in deuterated chloroform ($CDCl_3$). Before analysis, phase and baseline corrections were applied to all spectra, and the solvent peak was calibrated at 7.26 ppm.

SEC Analysis of the p(HexMA-PEGMA) Copolymer. The p(HexMA-PEGMA) copolymer was dissolved in tetrahydrofuran (THF) at a concentration of 5 mg/mL. A 50 μL aliquot of the solution was injected into a Shimadzu Prominence-i LC-2030C HPLC system equipped with SEC columns and operated with THF as the mobile phase at a flow rate of 0.7 mL/min. A differential refractive index (dRI) detector (model T-Rex, Wyatt Technology) was used for detection. The SEC columns were calibrated using polystyrene standards, and data analysis was performed using the conventional calibration method with Astra 6.1 software.

Preparation of the NGs. The copolymer was dissolved in 1 mL of water at a concentration of 5 mg/mL in a glass vial equipped with a magnetic stirrer. The solution was heated in a 55 °C water bath for 10 min. Afterward, 100 μL of an aqueous TA solution (500 mg/mL) was added to the copolymer solution, which was stirred for an additional minute at the same temperature. The mixture was then purified by dialysis against water for 24 h using a 12 kDa MWCO dialysis bag to remove any unbound TA. This procedure was followed to prepare all NGs with varying TA ratios.

TEM Analysis of TA Cross-Linked NGs. The NGs were diluted 10 times in Milli-Q water, and 4 μL of the diluted solution was dropped onto a TEM grid (Electron Microscopy Sciences, Formvar/Carbon 200 Mesh, Copper). After drying overnight, the sample was imaged using a T12 Quick room temperature TEM with 120 kV electron-beam energy. ImageJ software was used to analyze the size distribution of the NGs.

Hydrodynamic Size and Zeta Potential Characterizations of the NGs. The size of the NGs, diluted 10 times in Milli-Q water, was measured using DLS on a Malvern Zetasizer Nano-Z instrument (Malvern Instruments, Malvern, UK). Each sample was measured three times under standard operating conditions (25 °C with a 30-s equilibration time). Standard deviations reflected variability across repeated measurements. The zeta potential of the NGs was also determined using a disposable folded capillary cell (DTS1070) on the same instrument, with three measurements taken per sample following standard operating procedures.

FTIR of the Copolymer, NGs, and TA. FTIR analysis of the p(HexMA-PEGMA), the NGs, and TA was performed using a PerkinElmer Spectrum Two FTIR spectrometer in the frequency range of 500−4000 cm^{-1}. The engineered NG samples and synthesized p(HexMA-PEGMA) copolymer were freeze-dried before measurements, while commercially available TA was directly used for FTIR analysis. A small amount of each sample (2−5 mg) was directly placed onto the attenuated total reflectance (ATR) crystal and pressed down using the swivel press before FTIR measurements.

Turbidimetric Mucoadhesion Assessment of NGs. Mucin solutions of varying concentrations (0.25, 0.5, and 1.0 mg/mL) were prepared by dissolving mucin in 1 mL of DPBS with 2 h of magnetic stirring, followed by 30 min of sonication. Then, 20 μL of the NG solution (5 mg/mL) was added to 100 μL of the prepared mucin solution, vortexed vigorously for 30 s, and incubated at 37 °C for 10 min. The absorbance of the NG + mucin mixture was measured at 600 nm using UV−vis spectroscopy. The contribution of NGs to absorbance was subtracted before plotting the absorbance vs mucin concentration curve. Mucin solutions mixed with 20 μL of DPBS served as the control group.

Mucoadhesion Assessment of NGs by AFM. A mucin solution at a concentration of 1 mg/mL was prepared and coated onto Muscovite Mica (Electron Microscopy Sciences, US) using spin coating at 1000 rpm for 1 min. The coated mica surfaces were then dried under vacuum. For the mucoadhesion experiments, 1:3 NGs, 1:10 NGs, the copolymer (5 mg/mL), and DPBS were applied to the mucin-coated mica surfaces and spin-coated at 1000 rpm for 1 min. The mica surfaces were washed three times with Milli-Q water and dried in a desiccator overnight before AFM measurements. Imaging was performed in the air using the fast scanned mode on Bruker DimensionFastScan Atomic Force Microscope with ScanAsyst, at a scan rate of 0.901 Hz and a scan size of 20 μm.

Determination of DPPH• Scavenging Activity of NGs. Ten μL of NG dispersion (5 mg/mL) in water was mixed with ethanol solution of DPPH• (3 mL, 0.2 mM) and incubated at 25 °C for 5 min. The absorbance of the mixture at 517 nm was recorded using UV−vis spectroscopy. The radical scavenging activity of the p(HexMA-PEGMA) copolymer was also evaluated using the same concentration of the copolymer (5 mg/mL). The DPPH• solution in ethanol served as a control. The percentage of DPPH• scavenging activity was calculated using eq 2

$$\text{DPPH}\bullet\ \text{scavenging activity}\ (\%) = \frac{A_{\text{control}} - A_{\text{sample}}}{A_{\text{control}}} \times 100 \quad (2)$$

In the formula, $A_{control}$ represents the absorbance of DPPH• ethanol solution after 5 min incubation, while A_{sample} is the absorbance of the DPPH• solution mixed with NGs or the copolymer.

Assessment of MFX Loading Efficiency. MFX-loaded NGs were prepared by mixing the drug and copolymer in water, followed by heating the mixture to 55 °C and adding TA as a cross-linker. The resulting NG solution was then centrifuged using Amicon Ultra Centrifugal Filter (10 kDa MWCO) at 5,000 rpm for 30 min. After centrifugation, the solution was collected, and its absorbance was measured at 292 nm using UV−vis spectroscopy. Since TA also absorbs at 292 nm, its absorbance was subtracted from that of the unloaded drug solutions. To determine TA's absorbance, NGs without drug loading were used. Standard MFX solutions of varying concentrations were prepared in Milli-Q water via serial dilutions, and a calibration curve was generated from the absorbances of these MFX solutions. The amount of MFX loaded into the NGs was calculated using eq 3

$$\text{Loading Efficiency}\ (\%) = \frac{C_{\text{total}} - C_{\text{unloaded}}}{C_{\text{total}}} \times 100 \quad (3)$$

In the formula, C_{total} represents the total amount of MFX used for loading, while $C_{unloaded}$ refers to the free MFX measured in the solution.

Assessment of Dex Loading Efficiency and Drug Release Profile. The Dex loading was achieved by mixing 1 mL of Dex solution in acetone with 1 mL of copolymer solution, then heated to 55 °C until all acetone evaporated. TA cross-linking was subsequently performed. The unloaded drug was collected by centrifugation of the NG solution at 1,000 rpm for 5 min, which caused Dex to precipitate while the drug-loaded NGs remained in the solution. The precipitated Dex was dissolved in acetonitrile (ACN) and analyzed by high-performance liquid chromatography (HPLC) to quantify the amount of unloaded drug using a standard curve obtained from Dex solutions in ACN at various concentrations. Finally, the loading efficiency of Dex into the NGs was calculated using eq 3. The releasing profile of Dex from NGs was assessed using a dialysis method.[96] 0.9 mL of Dex-loaded NG solution was pipetted into a dialysis cup (Slide-A-Lyzer MINI Dialysis Devices, 20 kDa MWCO, Thermo Fisher Scientific). The dialysis cup was immersed in 14 mL of the releasing medium (DPBS) with stirring at 80 rpm at 37 °C. Samples (0.5 mL) of the receiving medium were drawn periodically, and 0.5 mL of fresh releasing medium were added back to keep the volume constant. The concentration of Dex in the different samples was measured using HPLC method mentioned previously.

Rheology Characterization of NGs and Dex Loaded NGs. The rheology of the NGs and Dex-loaded NGs was characterized using Discovery HR30. The results were obtained by linking the

https://doi.org/10.1021/acsnano.5c02002
ACS Nano 2025, 19, 27173−27191

measuring system Peltier plate Stainless steel (33868) with a diameter of 25 mm to the rheometer. Each measurement was carried out by loading a fresh sample in the 0.75 mm gap between the parallel plates and removing excessive samples. At a given shear rate parameter, ranging from 1 to 1000 s^{-1} with 60 measuring points at 37 °C, the relationship of viscosity and shear stress as a function of shear rate was recorded.

***In Vitro* Cytocompatibility Assay.** The cytocompatibility of engineered NGs was evaluated using NIH 3T3 fibroblasts for *in vitro* viability and metabolic activity assays. Live/Dead viability kits (Invitrogen) and Actin/DAPI staining were used to assess cell viability and proliferation, respectively, while the metabolic activity was measured using a Prestoblue assay (Life Sciences). NIH 3T3 cells were seeded at a density of 2×10^4 cells/well in 48-well plates, with 300 μL of DMEM growth medium added to each well along with 5 μL of NGs at different ratios (1:3 and 1:10 NGs). Plates were incubated at 37 °C in a humidified 5% CO_2 atmosphere for 5 days, with culture medium and NGs being replaced every 48 h.

Cell viability was evaluated using a Live/Dead viability kit (n = 4) according to the manufacturer's protocol. Cells were stained with 0.5 μL/mL calcein AM and 2 μL/mL ethidium homodimer-1 (EthD-1) in DPBS for 20 min at 37 °C. Fluorescent images were taken on days 1 and 5 postseeding using a Zeiss Axio Observer Z7 microscope. Viable (green) and dead (red) cells were quantified using ImageJ, and viability was determined as the number of live cells divided by the total number of cells. F-actin and nuclei were stained to visualize cell spreading. On days 1 and 5 postseeding, cells were fixed in 4% (v/v) paraformaldehyde for 15 min, permeabilized with 0.1% (w/v) Triton X-100 for 5 min, and blocked with 1% (w/v) BSA for 30 min. Samples were stained with Alexa Fluor 488 phalloidin for 45 min, followed by DAPI counterstaining. Imaging was performed using an inverted fluorescence microscope (Zeiss Axio Observer Z7).

PrestoBlue assays were performed on days 1, 3, and 7 postseeding (n = 6). Cells were incubated in 200 μL of 10% (v/v) PrestoBlue reagent in the growth medium for 45 min at 37 °C, and fluorescence was measured using a Synergy HT plate reader (BioTek).

***In Vitro* Intracellular ROS Scavenging Activity.** NIH 3T3 cells were cultured in 48-well plates for 24 h (3×10^4 cells/well). First, H_2O_2 solutions (50 μmol/L) were added to the cell culture medium to activate cells. After 25 min, the cell culture medium containing H_2O_2 was replaced by the cell culture medium (300 μL) containing NGs (2 and 5 μL) and incubated for 30 min. Lastly, the cell culture medium was replaced by a cell medium containing DCFH-DA solutions (100 μmol/L) and was incubated for 30 min. The green fluorescence signals in cells were studied by a fluorescence microscope (Olympus, IX71), and the fluorescence intensity was analyzed by ImageJ.

***In Vitro* Anti-Inflammation Assay.** RAW 264.7 cells in culture medium were inoculated in 48-well plates (3×10^4 cells/well) and cultured for 24 h. Then, macrophages were induced by adding 4 μg/mL LPS for 24 h. Then, NGs (1 and 2 μL) were added to the media for 48 h to exert anti-inflammatory effects. The expression of M1 phenotypic marker CD80 was detected by fluorescent microscope to determine the anti-inflammatory effects of the NGs. In short, after the macrophages were treated according to the above method, the cells experienced immobilization of 4% paraformaldehyde for 10 min. After PBS washing, 5% goat serum solution was used to block the cells for 1 h at room temperature. After PBS washing, the cells were incubated with an anti-CD80 antibody (diluted in 5% goat serum) for 2 h. After washing with PBS, the DAPI staining solution was adopted for nuclei imaging. Finally, the cells were observed and photographed under a fluorescent microscope (Zeiss Axio Observer Z7).

Assessment of BSA Loading Efficiency and Release. BSA loading was performed by mixing 0.5% BSA with the copolymer in DPBS, followed by heating the mixture to 50 °C. TA was then added as a cross-linker. The resulting NG solution was centrifuged, and the supernatant was collected for analysis. A BCA assay was conducted to quantify BSA content, measuring optical density OD at 562 nm using a TECAN M200 Pro plate reader.[97] To account for any background interference from TA, a control experiment was performed using NGs without BSA. Standard BSA solutions of different concentrations were prepared via serial dilutions in DPBS, and a calibration curve was generated based on their OD values. The amount of BSA loaded into the NGs was determined using eq 3. The release profile of BSA was evaluated using a dialysis method. 1 mL aliquot of BSA-loaded NG solution was placed in a dialysis tube (300 kDa MWCO) and immersed in 30 mL of release medium (DPBS), which was stirred at 80 rpm at 37 °C. Periodically, the release medium was sampled, and an equal volume of fresh DPBS was added. The concentration of released BSA was determined using a bicinchoninic acid (BCA) protein assay.[97] Hydrodynamic size and zeta potential of BSA-loaded NGs were measured by DLS using a Malvern Zetasizer Nano-Z instrument, as previously described.

Mice and Ethics Statement. C57BL/6 wild-type (WT) mice were purchased from Jackson Laboratory (Bar Harbor, ME) and maintained at the University of Missouri School of Medicine Office of Animal Resources (OAR) facility. Both male and female mice aged 6−10 weeks were used for all experiments. All animals were housed in a controlled access, The Association for Assessment and Accreditation of Laboratory Animal Care (AAALAC) approved, OAR facility, maintained in a 12:12 h light/dark cycle, and fed on lab diet rodent chow (Labdiet Pico Laboratory, Saint Louis, MO) and water ad libitum. Mice were treated in compliance with the Association for Research in Vision and Ophthalmology (ARVO) Statement for the Use of Animals in Ophthalmic and Vision Research.

Induction of Intraocular Inflammation. WT mice were anesthetized using ketamine (70 mg/kg) and xylazine (10 mg/kg) and intravitreally injected with LPS (100 ng/eye) using a 34-G needle under a dissecting microscope inside a biosafety cabinet. Contralateral eyes were injected with sterile PBS and used as controls. The animals were randomly divided into four groups: (i) LPS injection only, (ii) LPS injection with blank NGs treatment, (iii) LPS injection with Dex-loaded NGs treatment, and (iv) LPS injection with Dex solution (free drug) treatment. Animals were treated topically, 6 h post-LPS injection, either with blank NGs or Dex-loaded NGs or Dex solution for 48 h. Following treatment, the retinal tissue was harvested and subjected to qRT-PCR to measure the mRNA expression of proinflammatory cytokines/chemokines and genes modulating ROS production. From another set of experiments, eyes cryosections were used for histological analysis by H&E staining and SOD-2 and 8-OHdG immunofluorescence staining.

RNA Extraction and qRT-PCR. Total RNA was extracted from retinal tissue using TRIzol reagent per manufacturer's instructions (Thermo Scientific, Rockford, IL). Complementary DNA (cDNA) was synthesized using 1 μg of total RNA using a Maxima first-strand cDNA synthesis kit, per the manufacturer's instructions (Thermo Scientific, Rockford, IL). The cDNA was amplified using gene-specific PCR primers using QuantStudio 3 Real-Time PCR system (Thermo Fisher Scientific, Rockford, IL). The relative expression of genes was normalized in proportion to the constitutive gene 18s RNA as an internal control and quantitatively analyzed using the $\Delta\Delta_{CT}$ method and represented as fold change expression. The primers used for gene amplification are listed in Table S1.

Immunofluorescence Staining. For immunostaining, 10 μm-thick retinal sections were fixed with 4% paraformaldehyde in PBS for 15 min at room temperature. After three PBS washes, the sections were blocked and permeabilized using 10% (v/v) goat serum containing 0.4% Triton X-100 diluted in PBS for 2 h at room temperature. The retinal sections were then incubated with primary (anti-SOD2/8-OHdG) mouse/rabbit monoclonal antibodies (1:100 dilution) overnight at 4 °C. Following incubation, the sections were washed extensively with PBS and incubated with antimouse/rabbit Alexa Fluor 488/594-conjugated secondary antibody (1:200 dilution) for 1 h at room temperature. Tissue sections were extensively washed with PBS and mounted in Vectashield antifade mounting medium containing DAPI (Vector Laboratories, Burlingame, CA). The slides were imaged using a Keyence microscope (Keyence, Itasca, IL).

Histological Analysis. Following euthanasia, the eyes were enucleated and fixed using a modified Davidson's fixative. The embedding, sectioning, and H&E staining were performed by

https://doi.org/10.1021/acsnano.5c02002
ACS Nano 2025, 19, 27173−27191

Excalibur Pathology, Inc. (Norman, OK, USA). The slides were visualized and imaged using Keyence microscope (Keyence, Itasca, IL).

Statistical Analysis. Quantitative data were presented as mean ± standard error of mean (SEM), and significance levels are denoted as follows: $*p < 0.05$, $**p < 0.01$, $***p < 0.001$, and $****p < 0.0001$. Comparisons between multiple groups were conducted using the GraphPad Prism 8.4.3 software with a one-way ANOVA test. Each experiment included a minimum of three samples.

ASSOCIATED CONTENT

Supporting Information

The Supporting Information is available free of charge at https://pubs.acs.org/doi/10.1021/acsnano.5c02002.

Hydrodynamic size, PDI and zeta potential of 1:20 NGs, UV−vis spectrum and calibration curve of TA solutions at different concentrations, FTIR spectrum and turbidity curves of all NG solutions, SEC curve of p(HexMA-PEGMA) copolymer, surface roughness parameters from AFM analysis in mucoadhesion experiments, DPPH• scavenging activities and corresponding UV spectra of all NGs, accumulated release percentage of Dex from NGs, rheology characterization of 1:10 NG and Dex-loaded NG solutions, MFX loading efficiency, zeta potential measurements, hydrodynamic sizes and PDIs of NGs with varying MFX concentrations, and accumulated release percentage of BSA from NGs (PDF)

AUTHOR INFORMATION

Corresponding Author

Nasim Annabi − *Department of Chemical and Biomolecular Engineering, University of California, Los Angeles, California, Los Angeles 90095, United States; Department of Bioengineering, University of California, Los Angeles, California, Los Angeles 90095, United States;* orcid.org/0000-0003-1879-1202; Email: nannabi@ucla.edu

Authors

Yavuz Oz − *Department of Chemical and Biomolecular Engineering, University of California, Los Angeles, California, Los Angeles 90095, United States;* orcid.org/0000-0002-3862-4420

Yuting Zheng − *Department of Chemical and Biomolecular Engineering, University of California, Los Angeles, California, Los Angeles 90095, United States*

Prince Kumar − *Department of Ophthalmology, Mason Eye Institute, University of Missouri School of Medicine, Columbia, Missouri 65201, United States*

Lal Krishan Kumar − *Department of Ophthalmology, Mason Eye Institute, University of Missouri School of Medicine, Columbia, Missouri 65201, United States*

Arpita Roy − *Department of Chemical and Biomolecular Engineering, University of California, Los Angeles, California, Los Angeles 90095, United States;* orcid.org/0009-0008-6224-1471

Iris Qi − *Department of Life Sciences, University of California, Los Angeles, California, Los Angeles 90095, United States*

Zhanpeng Jim Liu − *Department of Chemical and Biomolecular Engineering, University of California, Los Angeles, California, Los Angeles 90095, United States*

Pawan Kumar Singh − *Department of Ophthalmology, Mason Eye Institute, University of Missouri School of Medicine, Columbia, Missouri 65201, United States*

Complete contact information is available at: https://pubs.acs.org/10.1021/acsnano.5c02002

Author Contributions

#Y.O. and Y.Z. contributed equally to this work.

Notes

The authors declare the following competing financial interest(s): Prof Annabi hold equity in GelMEDIX Inc.

ACKNOWLEDGMENTS

We acknowledge I. Martini for helping with the SEC experiment. This work was supported by the Department of Defense (DOD), Vision Research Program (VRP), Investigator Initiated Research Award (W81XWH-21-1-0869). This study was also supported in part by the National Institute of Health (NIH)/National Eye Institute (NEI) grant R01EY032495 and research start-up funds from the University of Missouri School of Medicine to P. K. Singh. The Table of Contents figure was created with BioRender.com.

REFERENCES

(1) Zhang, Y.; Li, S.; Loch, K.; Duncan, G. A.; Kaler, L.; Pangeni, R.; Peng, W.; Wang, S.; Gong, X.; Xu, Q. PH-Responsive Mucus-Penetrating Nanoparticles for Enhanced Cellular Internalization by Local Administration in Vaginal Tissue. *ACS Macro Lett.* **2023**, *12*, 446−453.

(2) Huang, K.; Guo, R.; Luo, H.; Liu, H.; Chen, D.; Deng, T.; Li, J.; He, J.; Xu, Z.; Li, M.; He, Q. Mucoadhesive Liposomal Delivery System Synergizing Anti-Inflammation and Anti-Oxidation for Enhanced Treatment against Dry Eye Disease. *J. Controlled Release* **2024**, *368*, 318−328.

(3) Huang, Q.-X.; Liang, J.-L.; Yang, C.-H.; Li, K.; Niu, M.-T.; Fan, J.-X.; Zhang, X.-Z. Stimulation-Responsive Mucoadhesive Probiotics for Inflammatory Bowel Disease Treatment by Scavenging Reactive Oxygen Species and Regulating Gut Microbiota. *Biomaterials* **2023**, *301*, 122274.

(4) Wang, X.; Yan, J.-J.; Wang, L.; Pan, D.; Yang, R.; Xu, Y.; Sheng, J.; Huang, Q.; Zhao, H.; Yang, M. Rational Design of Polyphenol-Poloxamer Nanovesicles for Targeting Inflammatory Bowel Disease Therapy. *Chem. Mater.* **2018**, *30*, 4073−4080.

(5) Lee, V. H. L.; Robinson, J. R. Topical Ocular Drug Delivery: Recent Developments and Future Challenges. *J. Ocul. Pharmacol. Ther.* **1986**, *2*, 67−108.

(6) Sun, X.; Sheng, Y.; Li, K.; Sai, S.; Feng, J.; Li, Y.; Zhang, J.; Han, J.; Tian, B. Mucoadhesive Phenylboronic Acid Conjugated Chitosan Oligosaccharide-Vitamin E Copolymer for Topical Ocular Delivery of Voriconazole: Synthesis, in Vitro/Vivo Evaluation, and Mechanism. *Acta Biomater* **2022**, *138*, 193−207.

(7) Li, C.; Liu, Z.; Yan, X.; Lu, W.; Liu, Y. Mucin-Controlled Drug Release from Mucoadhesive Phenylboronic Acid-Rich Nanoparticles. *Int. J. Pharm.* **2015**, *479*, 261−264.

(8) Liu, S.; Jones, L.; Gu, F. X. Development of Mucoadhesive Drug Delivery System Using Phenylboronic Acid Functionalized Poly (D, L-lactide)-b-dextran Nanoparticles. *Macromol. Biosci.* **2012**, *12*, 1622−1626.

(9) Menzel, C.; Bonengel, S.; de Sousa, I. P.; Laffleur, F.; Prüfert, F.; Bernkop-Schnürch, A. Preactivated Thiolated Nanoparticles: A Novel Mucoadhesive Dosage Form. *Int. J. Pharm.* **2016**, *497*, 123−128.

(10) Bradley, J.; Ju, M.; Robinson, G. S. Combination Therapy for the Treatment of Ocular Neovascularization. *Angiogenesis* **2007**, *10*, 141−148.

(11) Neamtu, I.; Rusu, A. G.; Diaconu, A.; Nita, L. E.; Chiriac, A. P. Basic Concepts and Recent Advances in Nanogels as Carriers for Medical Applications. *Drug Delivery* **2017**, *24*, 539−557.

(12) Oh, J. K.; Drumright, R.; Siegwart, D. J.; Matyjaszewski, K. The Development of Microgels/Nanogels for Drug Delivery Applications. *Prog. Polym. Sci.* **2008**, *33*, 448−477.

(13) Jiang, Y.; Chen, J.; Deng, C.; Suuronen, E. J.; Zhong, Z. C. H. Microgels and Nanogels: Emerging Platforms for Drug Delivery and Tissue Engineering. *Biomaterials* **2014**, *35*, 4969−4985.
(14) Ilka, R.; Mohseni, M.; Kianirad, M.; Naseripour, M.; Ashtari, K.; Mehravi, B. Nanogel-Based Natural Polymers as Smart Carriers for the Controlled Delivery of Timolol Maleate through the Cornea for Glaucoma. *Int. J. Biol. Macromol.* **2018**, *109*, 955−962.
(15) Silva Nieto, R.; Samaniego López, C.; Moretton, M. A.; Lizarraga, L.; Chiappetta, D. A.; Alaimo, A.; Pérez, O. E. Chitosan-Based Nanogels Designed for Betanin-Rich Beetroot Extract Transport: Physicochemical and Biological Aspects. *Polymers* **2023**, *15*, 3875.
(16) Zoratto, N.; Forcina, L.; Matassa, R.; Mosca, L.; Familiari, G.; Musarò, A.; Mattei, M.; Coviello, T.; Di Meo, C.; Matricardi, P. Hyaluronan-Cholesterol Nanogels for the Enhancement of the Ocular Delivery of Therapeutics. *Pharmaceutics* **2021**, *13*, 1781.
(17) Jahan, F.; Zaman, S. U.; Akhtar, S.; Arshad, R.; Ibrahim, I. M.; Shahnaz, G.; Rahdar, A.; Pandey, S. Development of Mucoadhesive Thiomeric Chitosan Nanoparticles for the Targeted Ocular Delivery of Vancomycin against Staphylococcus Aureus Resistant Strains. *Nanofabrication* **2021**, *6*, 16−24.
(18) Armengol, E. S.; Grassiri, B.; Piras, A. M.; Zambito, Y.; Fabiano, A.; Laffleur, F. Ocular Antibacterial Chitosan-Maleic Acid Hydrogels: In Vitro and in Vivo Studies for a Promising Approach with Enhanced Mucoadhesion. *Int. J. Biol. Macromol.* **2024**, *254*, 127939.
(19) Springsteen, G.; Wang, B. A Detailed Examination of Boronic Acid−Diol Complexation. *Tetrahedron* **2002**, *58*, 5291−5300.
(20) Huang, W.; Wu, X.; Gao, X.; Yu, Y.; Lei, H.; Zhu, Z.; Shi, Y.; Chen, Y.; Qin, M.; Wang, W.; Cao, Y. Maleimide−Thiol Adducts Stabilized through Stretching. *Nat. Chem.* **2019**, *11*, 310−319.
(21) Kirchhof, S.; Strasser, A.; Wittmann, H.-J.; Messmann, V.; Hammer, N.; Goepferich, A. M.; Brandl, F. P. New Insights into the Cross-Linking and Degradation Mechanism of Diels−Alder Hydrogels. *J. Mater. Chem. B* **2015**, *3*, 449−457.
(22) Zheng, Y.; Oz, Y.; Gu, Y.; Ahamad, N.; Shariati, K.; Chevalier, J.; Kapur, D.; Annabi, N. Rational Design of Polymeric Micelles for Targeted Therapeutic Delivery. *Nano Today* **2024**, *55*, 102147.
(23) Laradji, A. M.; Kolesnikov, A. V.; Karakoçak, B. B.; Kefalov, V. J.; Ravi, N. Redox-Responsive Hyaluronic Acid-Based Nanogels for the Topical Delivery of the Visual Chromophore to Retinal Photoreceptors. *ACS Omega* **2021**, *6*, 6172−6184.
(24) Abd El-Rehim, H. A.; Swilem, A. E.; Klingner, A.; Hegazy, E.-S. A.; Hamed, A. A. Developing the Potential Ophthalmic Applications of Pilocarpine Entrapped into Polyvinylpyrrolidone−Poly (Acrylic Acid) Nanogel Dispersions Prepared by γ Radiation. *Biomacromolecules* **2013**, *14*, 688−698.
(25) Nakai, T.; Hirakura, T.; Sakurai, Y.; Shimoboji, T.; Ishigai, M.; Akiyoshi, K. Injectable Hydrogel for Sustained Protein Release by Salt-induced Association of Hyaluronic Acid Nanogel. *Macromol. Biosci.* **2012**, *12*, 475−483.
(26) Shin, M.; Kim, K.; Shim, W.; Yang, J. W.; Lee, H. Tannic Acid as a Degradable Mucoadhesive Compound. *ACS Biomater. Sci. Eng.* **2016**, *2*, 687−696.
(27) Han, J. P.; Nam, Y. R.; Chung, H. Y.; Lee, H.; Yeom, S. C. Polyphenol-Enabled 2D Nanopatch for Enhanced Nasal Mucoadhesion and Immune Activation. *Nano Lett.* **2024**, *24*, 10380−10387.
(28) Feng, G.; Han, K.; Yang, Q.; Feng, W.; Guo, J.; Wang, J.; Yang, X. Interaction of Pyrogallol-Containing Polyphenols with Mucin Reinforces Intestinal Mucus Barrier Properties. *J. Agric. Food Chem.* **2022**, *70*, 9536−9546.
(29) Nita, M.; Grzybowski, A. The Role of the Reactive Oxygen Species and Oxidative Stress in the Pathomechanism of the Age-Related Ocular Diseases and Other Pathologies of the Anterior and Posterior Eye Segments in Adults. *Oxid. Med. Cell. Longev.* **2016**, *2016*, 3164734.
(30) Ung, L.; Pattamatta, U.; Carnt, N.; Wilkinson-Berka, J. L.; Liew, G.; White, A. J. R. Oxidative Stress and Reactive Oxygen Species: A Review of Their Role in Ocular Disease. *Clin. Sci.* **2017**, *131*, 2865−2883.
(31) Kaarniranta, K.; Pawlowska, E.; Szczepanska, J.; Jablkowska, A.; Blasiak, J. Role of Mitochondrial DNA Damage in ROS-Mediated Pathogenesis of Age-Related Macular Degeneration (AMD). *Int. J. Mol. Sci.* **2019**, *20*, 2374.
(32) Kowluru, R. A.; Chan, P.-S. Oxidative Stress and Diabetic Retinopathy. *J. Diabetes Res.* **2007**, *2007*, 043603.
(33) Vinson, J. A. Oxidative Stress in Cataracts. *Pathophysiology* **2006**, *13*, 151−162.
(34) McMonnies, C. Reactive Oxygen Species, Oxidative Stress, Glaucoma and Hyperbaric Oxygen Therapy. *J. Optom.* **2018**, *11*, 3−9.
(35) Zhang, D.; He, J.; Hua, S. Y.; Li, Y.; Zhou, M. Reactive Oxygen Species-Responsive Dual Anti-Inflammatory and Antioxidative Nanoparticles for Anterior Uveitis. *ACS Appl. Mater. Interfaces* **2024**, *16*, 22850−22864.
(36) Balitaan, J. N. I.; Hsiao, C.-D.; Yeh, J.-M.; Santiago, K. S. Innovation Inspired by Nature: Biocompatible Self-Healing Injectable Hydrogels Based on Modified-β-Chitin for Wound Healing. *Int. J. Biol. Macromol.* **2020**, *162*, 723−736.
(37) Rahmani, S.; Barzegar, M. One-Pot Synthesis of Dibenzaldehyde-Terminated Poly (Ethylene Glycol) for Preparation of Dynamic Chitosan-Based Amphiphilic Hydrogels. *Polym. Bull.* **2021**, *78*, 2887−2909.
(38) Ohke, M.; Akaishi, R.; Tachibana, K.; Kohri, M.; Nagano, S.; Ebe, H.; Matsui, J. Janus Metallic Film with Gold and Silver Luster by Electroless Deposition of Silver Using Poly (Dopamine Acrylamide) Thin Film. *RSC Adv.* **2023**, *13*, 28104−28111.
(39) Li, B.; Whalen, J. J.; Humayun, M. S.; Thompson, M. E. Reversible Bioadhesives Using Tannic Acid Primed Thermally-responsive Polymers. *Adv. Funct. Mater.* **2020**, *30*, 1907478.
(40) Lutz, J. Polymerization of Oligo (Ethylene Glycol)(Meth) Acrylates: Toward New Generations of Smart Biocompatible Materials. *J. Polym. Sci., Part A: Polym. Chem.* **2008**, *46*, 3459−3470.
(41) Aktan, B.; Chambre, L.; Sanyal, R.; Sanyal, A. "Clickable" Nanogels via Thermally Driven Self-Assembly of Polymers: Facile Access to Targeted Imaging Platforms Using Thiol−Maleimide Conjugation. *Biomacromolecules* **2017**, *18*, 490−497.
(42) Chambre, L.; Saw, W. S.; Ekineker, G.; Kiew, L. V.; Chong, W. Y.; Lee, H. B.; Chung, L. Y.; Bretonnière, Y.; Dumoulin, F.; Sanyal, A. Surfactant-Free Direct Access to Porphyrin-Cross-Linked Nanogels for Photodynamic and Photothermal Therapy. *Bioconjugate Chem.* **2018**, *29*, 4149−4159.
(43) Ryu, J.-H.; Chacko, R. T.; Jiwpanich, S.; Bickerton, S.; Babu, R. P.; Thayumanavan, S. Self-Cross-Linked Polymer Nanogels: A Versatile Nanoscopic Drug Delivery Platform. *J. Am. Chem. Soc.* **2010**, *132*, 17227−17235.
(44) Almásy, L.; Artykulnyi, O. P.; Petrenko, V. I.; Ivankov, O. I.; Bulavin, L. A.; Yan, M.; Haramus, V. M. Structure and Intermolecular Interactions in Aqueous Solutions of Polyethylene Glycol. *Molecules* **2022**, *27*, 2573.
(45) Nagahama, K.; Hashizume, M.; Yamamoto, H.; Ouchi, T.; Ohya, Y. Hydrophobically Modified Biodegradable Poly (Ethylene Glycol) Copolymers That Form Temperature-Responsive Nanogels. *Langmuir* **2009**, *25*, 9734−9740.
(46) Peng, Q.; Wu, Q.; Chen, J.; Wang, T.; Wu, M.; Yang, D.; Peng, X.; Liu, J.; Zhang, H.; Zeng, H. Coacervate-Based Instant and Repeatable Underwater Adhesive with Anticancer and Antibacterial Properties. *ACS Appl. Mater. Interfaces* **2021**, *13*, 48239−48251.
(47) Park, J.; Park, E.; Choi, S. Q.; Wu, J.; Park, J.; Lee, H.; Kim, H.; Lee, H.; Seo, M. Biodegradable Block Copolymer−Tannic Acid Glue. *JACS Au* **2022**, *2*, 1978−1988.
(48) Liang, H.; Pei, Y.; Li, J.; Xiong, W.; He, Y.; Liu, S.; Li, Y.; Li, B. PH-Degradable Antioxidant Nanoparticles Based on Hydrogen-Bonded Tannic Acid Assembly. *RSC Adv.* **2016**, *6*, 31374−31385.
(49) Kwon, J.; Lee, H. Poly (Ethylene Glycol)(PEG)-Based Microgels Embedded with Magnetic Nanoparticles for Tannin Removal and Valorization. *Korean J. Chem. Eng.* **2023**, *40*, 445−451.
(50) Das Neves, J.; Bahia, M. F.; Amiji, M. M.; Sarmento, B. Mucoadhesive Nanomedicines: Characterization and Modulation of

https://doi.org/10.1021/acsnano.5c02002
ACS Nano 2025, 19, 27173−27191

Mucoadhesion at the Nanoscale. *Expert Opin. Drug Delivery* **2011**, *8*, 1085−1104.
(51) Oz, Y.; Arslan, M.; Gevrek, T. N.; Sanyal, R.; Sanyal, A. Modular Fabrication of Polymer Brush Coated Magnetic Nanoparticles: Engineering the Interface for Targeted Cellular Imaging. *ACS Appl. Mater. Interfaces* **2016**, *8*, 19813−19826.
(52) Kim, K.; Shin, M.; Koh, M.; Ryu, J. H.; Lee, M. S.; Hong, S.; Lee, H. TAPE: A Medical Adhesive Inspired by a Ubiquitous Compound in Plants. *Adv. Funct. Mater.* **2015**, *25*, 2402−2410.
(53) Zheng, Y.; Baidya, A.; Annabi, N. Molecular Design of an Ultra-Strong Tissue Adhesive Hydrogel with Tunable Multifunctionality. *Bioact. Mater.* **2023**, *29*, 214−229.
(54) Di Prima, G.; Bongiovì, F.; Palumbo, F. S.; Pitarresi, G.; Licciardi, M.; Giammona, G. Mucoadhesive PEGylated Inulin-Based Self-Assembling Nanoparticles: In Vitro and Ex Vivo Transcorneal Permeation Enhancement of Corticosteroids. *J. Drug Delivery Sci. Technol.* **2019**, *49*, 195−208.
(55) Račić, A.; Čalija, B.; Milić, J.; Milašinović, N.; Krajišnik, D. Development of Polysaccharide-Based Mucoadhesive Ophthalmic Lubricating Vehicles: The Effect of Different Polymers on Physicochemical Properties and Functionality. *J. Drug Delivery Sci. Technol.* **2019**, *49*, 50−57.
(56) Dave, R. S.; Goostrey, T. C.; Ziolkowska, M.; Czerny-Holownia, S.; Hoare, T.; Sheardown, H. Ocular Drug Delivery to the Anterior Segment Using Nanocarriers: A Mucoadhesive/Mucopenetrative Perspective. *J. Controlled Release* **2021**, *336*, 71−88.
(57) Lall, N.; Henley-Smith, C. J.; De Canha, M. N.; Oosthuizen, C. B.; Berrington, D. V. R. Viability Reagent, PrestoBlue, in Comparison with Other Available Reagents, Utilized in Cytotoxicity and Antimicrobial Assays. *Int. J. Microbiol.* **2013**, *2013*, 420601.
(58) Böhm, E. W.; Buonfiglio, F.; Voigt, A. M.; Bachmann, P.; Safi, T.; Pfeiffer, N.; Gericke, A. Oxidative Stress in the Eye and Its Role in the Pathophysiology of Ocular Diseases. *Redox Biol.* **2023**, *68*, 102967.
(59) Seen, S.; Tong, L. Dry Eye Disease and Oxidative Stress. *Acta Ophthalmol.* **2018**, *96*, No. e412−e420.
(60) Shoham, A.; Hadziahmetovic, M.; Dunaief, J. L.; Mydlarski, M. B.; Schipper, H. M. Oxidative Stress in Diseases of the Human Cornea. *Free Radical Biol. Med.* **2008**, *45*, 1047−1055.
(61) Liu, M.; Chen, J.; Li, L.; Zhou, J.; Narain, R.; Nan, K.; Chen, Y. Anti-Oxidative Tannic Acid-Based Nanogels Formed via Dynamic Benzoxaborolate Cross-Linking at Physiological PH. *J. Mol. Liq.* **2024**, *398*, 124239.
(62) Jiao, Z.; Huo, Q.; Lin, X.; Chu, X.; Deng, Z.; Guo, H.; Peng, Y.; Lu, S.; Zhou, X.; Wang, X.; Wang, B. Drug-Free Contact Lens Based on Quaternized Chitosan and Tannic Acid for Bacterial Keratitis Therapy and Corneal Repair. *Carbohydr. Polym.* **2022**, *286*, 119314.
(63) Bi, D.; Qu, F.; Xiao, W.; Wu, J.; Liu, P.; Du, H.; Xie, Y.; Liu, H.; Zhang, L.; Tao, J.; Liu, Y. Reactive Oxygen Species-Responsive Gel-Based Microneedle Patches for Prolonged and Intelligent Psoriasis Management. *ACS Nano* **2023**, *17*, 4346−4357.
(64) Jia, G.; Li, Z.; Le, H.; Jiang, Z.; Sun, Y.; Liu, H.; Chang, F. Green Tea Derivative-Based Hydrogel with ROS-Scavenging Property for Accelerating Diabetic Wound Healing. *Mater. Des.* **2023**, *225*, 111452.
(65) Jiang, Y.; Zhang, X.; Zhang, W.; Wang, M.; Yan, L.; Wang, K.; Han, L.; Lu, X. Infant Skin Friendly Adhesive Hydrogel Patch Activated at Body Temperature for Bioelectronics Securing and Diabetic Wound Healing. *ACS Nano* **2022**, *16*, 8662−8676.
(66) Thomas, M. L. R. M. G.; Barbosa Filho, J. M. Anti-Inflammatory Actions of Tannins Isolated from the Bark of Anacardium Occidentale L. *J. Ethnopharmacol.* **1985**, *13*, 289−300.
(67) Suri, R.; Beg, S.; Kohli, K. Target Strategies for Drug Delivery Bypassing Ocular Barriers. *J. Drug Delivery Sci. Technol.* **2020**, *55*, 101389.
(68) Torres-Luna, C.; Koolivand, A.; Fan, X.; Agrawal, N. R.; Hu, N.; Zhu, Y.; Domszy, R.; Briber, R. M.; Wang, N. S.; Yang, A. Formation of Drug-Participating Catanionic Aggregates for Extended Delivery of Non-Steroidal Anti-Inflammatory Drugs from Contact Lenses. *Biomolecules* **2019**, *9*, 593.
(69) Sahiner, N.; Sagbas, S.; Aktas, N.; Silan, C. Inherently Antioxidant and Antimicrobial Tannic Acid Release from Poly (Tannic Acid) Nanoparticles with Controllable Degradability. *Colloids Surf., B* **2016**, *142*, 334−343.
(70) Shagholani, H.; Ghoreishi, S. M. Investigation of Tannic Acid Cross-Linked onto Magnetite Nanoparticles for Applying in Drug Delivery Systems. *J. Drug Delivery Sci. Technol.* **2017**, *39*, 88−94.
(71) Zhao, Y.-N.; Gu, J.; Jia, S.; Guan, Y.; Zhang, Y. Zero-Order Release of Polyphenolic Drugs from Dynamic, Hydrogen-Bonded LBL Films. *Soft Matter.* **2016**, *12*, 1085−1092.
(72) Jossic, L.; Lefevre, P.; de Loubens, C.; Magnin, A.; Corre, C. The Fluid Mechanics of Shear-Thinning Tear Substitutes. *J. Nonnewton. Fluid Mech.* **2009**, *161*, 1−9.
(73) Adler, C. A.; Maurice, D. M.; Paterson, M. E. The Effect of Viscosity of the Vehicle on the Penetration of Fluorescein into the Human Eye. *Exp. Eye Res.* **1971**, *11*, 34−42.
(74) Abadia, B.; Calvo, P.; Ferreras, A.; Bartol, F.; Verdes, G.; Pablo, L. Clinical Applications of Dexamethasone for Aged Eyes. *Drugs Aging* **2016**, *33*, 639−646.
(75) Caban, M.; Owczarek, K.; Chojnacka, K.; Lewandowska, U. Overview of Polyphenols and Polyphenol-Rich Extracts as Modulators of Inflammatory Response in Dry Eye Syndrome. *Food Rev. Int.* **2022**, *38* (sup1), 501−528.
(76) Yeo, J.; Lee, J.; Yoon, S.; Kim, W. J. Tannic Acid-Based Nanogel as an Efficient Anti-Inflammatory Agent. *Biomater. Sci.* **2020**, *8*, 1148−1159.
(77) Mandal, A.; Pal, D.; Agrahari, V.; Trinh, H. M.; Joseph, M.; Mitra, A. K. Ocular Delivery of Proteins and Peptides: Challenges and Novel Formulation Approaches. *Adv. Drug Delivery Rev.* **2018**, *126*, 67−95.
(78) Kazemi, M. S.; Shoari, A.; Salehibakhsh, N.; Aliabadi, H. A. M.; Abolhosseini, M.; Arab, S. S.; Ahmadieh, H.; Kanavi, M. R.; Behdani, M. Anti-Angiogenic Biomolecules in Neovascular Age-Related Macular Degeneration; Therapeutics and Drug Delivery Systems. *Int. J. Pharm* **2024**, *659*, 124258.
(79) Silva, M.; Peng, T.; Zhao, X.; Li, S.; Farhan, M.; Zheng, W. Recent Trends in Drug-Delivery Systems for the Treatment of Diabetic Retinopathy and Associated Fibrosis. *Adv. Drug Delivery Rev.* **2021**, *173*, 439−460.
(80) Akhtar-Schäfer, I.; Wang, L.; Krohne, T. U.; Xu, H.; Langmann, T. Modulation of Three Key Innate Immune Pathways for the Most Common Retinal Degenerative Diseases. *EMBO Mol. Med.* **2018**, *10* (10), No. e8259.
(81) Attia, S. A.; MacKay, J. A. Protein and Polypeptide Mediated Delivery to the Eye. *Adv. Drug Delivery Rev.* **2022**, *188*, 114441.
(82) El Sanharawi, M.; Kowalczuk, L.; Touchard, E.; Omri, S.; De Kozak, Y.; Behar-Cohen, F. Protein Delivery for Retinal Diseases: From Basic Considerations to Clinical Applications. *Prog. Retin. Eye Res.* **2010**, *29*, 443−465.
(83) Wykoff, C. C.; Clark, W. L.; Nielsen, J. S.; Brill, J. V.; Greene, L. S.; Heggen, C. L. Optimizing Anti-VEGF Treatment Outcomes for Patients with Neovascular Age-Related Macular Degeneration. *J. Manag. Care Spec. Pharm.* **2018**, *24* (2−a Suppl), S3−S15.
(84) Saadoun, D.; Bodaghi, B.; Bienvenu, B.; Wechsler, B.; Sene, D.; Trad, S.; Abad, S.; Cacoub, P.; Kodjikian, L.; Sève, P. Biotherapies in Inflammatory Ocular Disorders: Interferons, Immunoglobulins, Monoclonal Antibodies. *Autoim. Rev.* **2013**, *12*, 774−783.
(85) Mohamed, H. B.; Abd El-Hamid, B. N.; Fathalla, D.; Fouad, E. A. Current Trends in Pharmaceutical Treatment of Dry Eye Disease: A Review. *Eur. J. Pharm. Sci.* **2022**, *175*, 106206.
(86) Grzybowski, A.; Brockmann, T.; Kanclerz, P.; Pleyer, U. Dexamethasone Intraocular Suspension: A Long-Acting Therapeutic for Treating Inflammation Associated with Cataract Surgery. *J. Ocul. Pharmacol. Ther.* **2019**, *35*, 525−534.
(87) Hermans, H.; van den Berg, E. M. H.; Slenter, I. J. M.; Vendrig, D. J. C.; de nijs-Tjon, L. J. L.; Vernooij, J. C. M.; Brommer, H.; Boevé, M. H.; Gehring, R. Penetration of Topically Administered Dexa-

https://doi.org/10.1021/acsnano.5c02002
ACS Nano 2025, 19, 27173−27191

methasone Disodium Phosphate and Prednisolone Acetate into the Normal Equine Ocular Fluids. *Equine Vet. J.* **2022**, *54*, 965−972.
(88) Kumar, A.; Singh, P. K.; Ahmed, Z.; Singh, S.; Kumar, A.; Torres, V. J. Essential Role of NLRP3 Inflammasome in Mediating IL-1β Production and the Pathobiology of Staphylococcus Aureus Endophthalmitis. *Infect. Immun.* **2022**, *90* (5), No. e00103.
(89) Kumar, A.; Kumar, A. Role of Staphylococcus Aureus Virulence Factors in Inducing Inflammation and Vascular Permeability in a Mouse Model of Bacterial Endophthalmitis. *PLoS One* **2015**, *10*, No. e0128423.
(90) Kumar, A.; Singh, P. K.; Zhang, K.; Kumar, A. Toll-like Receptor 2 (TLR2) Engages Endoplasmic Reticulum Stress Sensor IRE1α to Regulate Retinal Innate Responses in S. Aureus Endophthalmitis. *FASEB J. Off. Publ. Fed. Am. Soc. Exp. Biol.* **2020**, *34*, 13826.
(91) Kim, H. M.; Woo, S. J. Ocular Drug Delivery to the Retina: Current Innovations and Future Perspectives. *Pharmaceutics* **2021**, *13*, 108.
(92) Bedard, K.; Krause, K.-H. The NOX Family of ROS-Generating NADPH Oxidases: Physiology and Pathophysiology. *Physiol. Rev.* **2007**, *87*, 245−313.
(93) Ighodaro, O. M.; Akinloye, O. A. First Line Defence Antioxidants-Superoxide Dismutase (SOD), Catalase (CAT) and Glutathione Peroxidase (GPX): Their Fundamental Role in the Entire Antioxidant Defence Grid. *Alexandria J. Med.* **2018**, *54*, 287−293.
(94) Valavanidis, A.; Vlachogianni, T.; Fiotakis, C. 8-Hydroxy-2′-Deoxyguanosine (8-OHdG): A Critical Biomarker of Oxidative Stress and Carcinogenesis. *J. Environ. Sci. Heal. Part C* **2009**, *27*, 120−139.
(95) Mahmoudi, Z.; Mohammadnejad, J.; Bazaz, S. R.; Mehrizi, A. A.; Saidijam, M.; Dinarvand, R.; Warkiani, M. E.; Soleimani, M. Promoted Chondrogenesis of HMCSs with Controlled Release of TGF-B3 via Microfluidics Synthesized Alginate Nanogels. *Carbohydr. Polym.* **2020**, *229*, 115551.
(96) Pepić, I.; Hafner, A.; Lovrić, J.; Pirkić, B.; Filipović-Grččić, J. A Nonionic Surfactant/Chitosan Micelle System in an Innovative Eye Drop Formulation. *J. Pharm. Sci.* **2010**, *99*, 4317−4325.
(97) Liu, C.; Wen, J.; Li, D.; Qi, H.; Nih, L.; Zhu, J.; Xu, D.; Ren, Y.; Zhang, S.; Han, D.; Jia, H. Systemic Delivery of MicroRNA for Treatment of Brain Ischemia. *Nano Res.* **2021**, *14*, 3319−3328.

https://doi.org/10.1021/acsnano.5c02002
ACS Nano 2025, 19, 27173−27191